

Banner appropriate to article type will appear here in typeset article

# The interplay of inertia and elasticity in polymeric flows

Rahul Kumar Singh and Marco Edoardo Rosti<sup>†</sup>

Complex Fluids and Flows Unit, Okinawa Institute of Science and Technology Graduate University (OIST), 1919-1 Tancha, Onna-son, Okinawa 904-0495, Japan

(Received xx; revised xx; accepted xx)

Addition of polymers modifies a turbulent flow in a manner that depends non-trivially on the interplay of fluid inertia, quantified by the Reynolds number  $Re$ , and the elasticity of the dissolved polymers, given by the Deborah number  $De$ . We use direct numerical simulations to study polymeric flows at different  $Re$  and  $De$  numbers, and uncover various features of their dynamics. Polymeric flows exhibit a multiscaling energy spectrum that is a function of  $Re$  and  $De$ , owing to different dominant contributions to the total energy flux across scales. This behaviour is also manifested in the real space scaling of structure functions. We also shed light on how the addition of polymers results in slowing down the fluid non-linear cascade resulting in a depleted flux, as velocity fluctuations with less energy persist for longer times in polymeric flows. These velocity fluctuations exhibit intermittent, large deviations similar to that in a Newtonian flow at large  $Re$ , but differ more and more as  $Re$  becomes smaller. This observation is further supported by the statistics of fluid energy dissipation in polymeric flows, whose distributions collapse on to the Newtonian at large  $Re$ , but increasingly differ from it as  $Re$  decreases. We also show that polymer dissipation is significantly less intermittent compared to fluid dissipation, and even less so when elasticity becomes large. Polymers, on an average, dissipate more energy when they are stretched more, which happens in extensional regions of the flow. However, owing to vortex stretching, regions with large rotation rates also correlate with large polymer extensions, albeit to a relatively less degree than extensional regions.

## 1. Introduction

Polymeric flows are very well known to give rise to a wide range of intriguing phenomena. The pioneering work by Toms (1948) showed that a small concentration of polymers added to a carrier flow results in the reduction of turbulent drag, which were reviewed in Lumley (1973); Virk (1975); Toms (1977) and Berman (1978). Ever since this discovery, there have been numerous theoretical (Tabor & de Gennes 1986; Bhattacharjee & Thirumalai 1991; Sreenivasan & White 2000; L'vov *et al.* 2004; Procaccia *et al.* 2008), numerical (Benzi *et al.* 2003; Kalelkar *et al.* 2005; Perlekar *et al.* 2006; White & Mungal 2008; Gillissen 2008; Choueiri *et al.* 2018; Xi 2019; Rosti *et al.* 2023) and experimental (Den Toonder *et al.* 1997; Escudier *et al.* 1999; Ptasinski *et al.* 2001, 2003; Yang & Dou 2010) works in an attempt to better understand and highlight its origins and the underlying mechanisms. Lumley (1973)

<sup>†</sup> Email address for correspondence: marco.rosti@oist.jp

and Hinch (1977) showed that dissolved polymers tend to increase the effective viscosity of a solution, however there can be a net reduction in the dissipation of energy in such turbulent, polymeric flows, as was pointed out by van Doorn *et al.* (1999); Kalelkar *et al.* (2005); Perlekar *et al.* (2006, 2010) and Cai *et al.* (2010). This rich, and complex behaviour of polymeric flows is dictated by an interplay of two intrinsic features: inertia and elasticity. Inertia is a property of the Newtonian, carrier flow, whose strength is determined by the non-dimensional Reynolds number  $Re$ . A large  $Re$  is typically indicative of a highly turbulent flow where flow structures span a wide range of scales. Elasticity, on the other hand, is a characteristic of the polymers, that determines their tendency to stretch and is quantified by the non-dimensional Deborah number  $De$ . A large  $De$  means the polymers take longer to relax back to their equilibrium lengths and remain stretched for longer times.

Experiments by Larson (1992); Shaqfeh (1996); Groisman & Steinberg (1998) and Pan *et al.* (2013) have shown that flows at small  $Re$  develop instabilities when polymers are added in small concentrations. At extremely small  $Re$ , when fluid non-linearity remains dormant, instabilities driven by purely elastic effects result in a flow state referred to as elastic turbulence (ET) which shows qualitatively similar behaviour to classical high  $Re$  turbulence (HIT) in many respects. These include the existence of a chaotic flow state, as illustrated in the works of Groisman & Steinberg (2000, 2004) and Qin & Arratia (2017), as well as enhancement of mixing Groisman & Steinberg (2001) and heat transfer Li *et al.* (2017). A self-similar distribution of kinetic energy over a wide range of scales was also observed in numerical simulations of ET (Berti *et al.* 2008; Berti & Boffetta 2010; Ray & Vincenzi 2016; Gupta & Vincenzi 2019; Singh *et al.* 2024; Rota *et al.* 2024; Lewy & Kerswell 2024). At larger, yet moderate  $Re$ , it is now known that polymer elasticity and the fluid non-linearity (albeit with a weaker contribution as shown by Gillissen (2021)) conspire to trigger a turbulence-like behaviour much earlier than that in a Newtonian flow (Dubief *et al.* 2013; Samanta *et al.* 2013; Valente *et al.* 2016; Dubief *et al.* 2023). Such a flow state at moderate  $Re$  is referred to as elasto-inertial turbulence (EIT). Fluid kinetic energy in EIT is also known to exhibit a distinct self-similar, scaling behaviour (Zhang *et al.* 2021a; Dubief *et al.* 2013; Valente *et al.* 2016). At very large  $Re$  numbers, turbulent polymeric flows (PHIT) exhibit a novel self-similar spectrum whose scaling exponents differ from those predicted by the Kolmogorov theory (K41) for classical Newtonian turbulence (HIT) (Kolmogorov 1941; Frisch 1996). This was uncovered recently in the experiments of Zhang *et al.* (2021b) as well as in the numerical simulations of Rosti *et al.* (2023).

In this work, we study turbulent polymeric flows in a triperiodic box across a wide range of  $Re$  and  $De$  numbers, and show how various aspects of their dynamics change with changing fluid inertia and elasticity. We show that the addition of polymers results in a multiscaling of the energy spectrum, that emerges as a result of different underlying dominant flux contributions. The fluxes furthermore reveal that polymers slow down the rate of energy transfer via the fluid non-linear cascade, signalling a weakened fluid non-linear cascade. We then discuss how polymers are, in turn, themselves affected by Newtonian carrier flow. In particular, we show that the polymers stretch in both the extensional and rotational regions of the flow, with the correlation being less for the latter. Both fluid and polymer extensions are directly related to the corresponding dissipations, which show contrasting characteristics. Fluid dissipation shows more large deviations about the mean at small  $Re$  and large  $De$ , while polymer dissipation is less intermittent, and even lesser at large  $De$ . We structure all of the above as follows: the details of numerical simulations are provided in the immediately following Section 2 before moving on to the results in Section 3. Finally, we summarise our conclusions in Section 4.

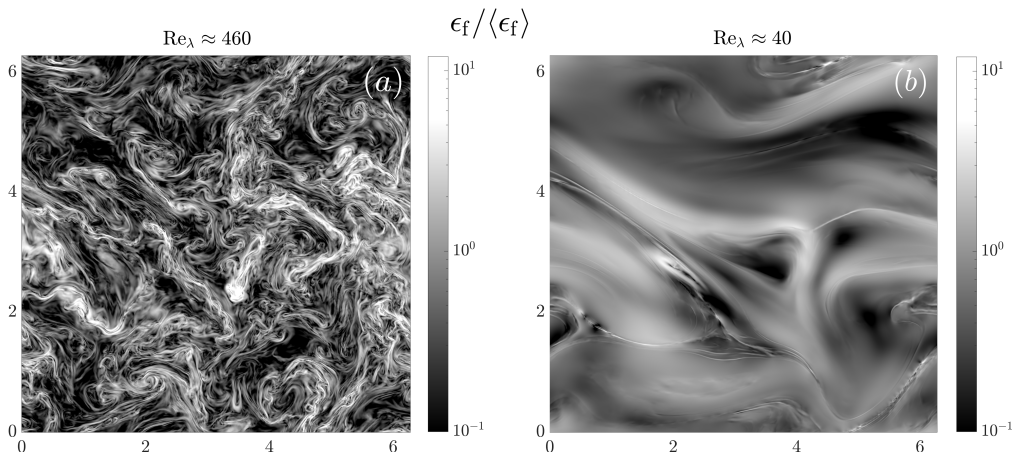


Figure 1: Representative snapshots of normalized fluid energy dissipation rates  $\epsilon_f$  at (a) large and (b) small  $Re$  for  $De \approx 1$ . Large  $Re_\lambda$  polymeric flows exhibit a wide range of flow structures, while the small  $Re_\lambda$  flows have only large scale structures.

## 2. Mathematical model and numerical method

We arrive at our results via the direct numerical simulations of polymeric flows that comprise an incompressible Newtonian carrier fluid whose dynamics is described by a velocity field  $\mathbf{u}$  ( $\nabla \cdot \mathbf{u} = 0$ ), with dissolved polymers that are described by a conformation tensor field  $\mathbf{C}$ . The trace of this conformation field  $\text{Tr}[\mathbf{C}] = C_{ii}$  (with  $i = 1, 2, 3$ ) is a measure of the instantaneous, squared end-to-end lengths of the polymers. In particular, we adopt the Oldroyd-B model of polymers, which has often been used to study polymeric flows in various settings in a number of works (Vincenzi *et al.* 2007; Berti *et al.* 2008; De Lillo *et al.* 2012; Bagheri *et al.* 2012; Gupta & Vincenzi 2019; Zhang *et al.* 2021a; Rosti *et al.* 2023). The flow is described by the simultaneous evolution of the coupled equations:

$$\rho (\partial_t \mathbf{u} + \mathbf{u} \cdot \nabla \mathbf{u}) = -\nabla p + \mu_s \nabla^2 \mathbf{u} + \frac{\mu_p}{\tau_p} \nabla \cdot \mathbf{C} + \mathbf{F}, \quad (2.1a)$$

$$\partial_t \mathbf{C} + \mathbf{u} \cdot \nabla \mathbf{C} = \mathbf{C} \nabla \mathbf{u} + (\nabla \mathbf{u})^T \mathbf{C} - \frac{1}{\tau_p} (\mathbf{C} - \mathbf{I}), \quad (2.1b)$$

where  $\rho$  is the fluid density,  $p$  the pressure,  $\mu_s$  the dynamic viscosity of the Newtonian fluid (kinematic viscosity  $\nu = \mu_s/\rho$ ),  $\mu_p$  the dynamic polymer viscosity, and  $\tau_p$  is the unique relaxation time of the polymers. A statistically stationary state is maintained by energy injection via the forcing  $\mathbf{F}$  for which we employ the ABC scheme such that  $\mathbf{F} = \nu[(A \sin z + C \cos y) \hat{\mathbf{x}} + (B \sin x + A \cos z) \hat{\mathbf{y}} + (C \sin y + B \cos x) \hat{\mathbf{z}}]$ , where  $A = B = C = 1$ . The total energy injected per unit time  $\epsilon_t$  is dissipated away by both the Newtonian fluid ( $\epsilon_f$ ) and the polymers ( $\epsilon_p$ ), such that  $\epsilon_t = \epsilon_f + \epsilon_p$ .

The flow is characterised by two dimensionless numbers: the Taylor-scale Reynolds number,  $Re_\lambda \equiv u_{rms} \lambda / \nu$ , where  $\lambda \equiv u_{rms} \sqrt{15 \nu / \epsilon_f}$  is the Taylor length scale and  $u_{rms}$  the root mean square velocity, and the Deborah number,  $De \equiv \tau_p / \tau_L$ , where  $\tau_L = L / u_{rms}$  is the large-eddy turnover time, with  $L$  being the scale of the forcing. We choose  $Re_\lambda \in \{40, 100, 240, 320, 460\}$  and  $De \in \{1/9, 1/3, 1, 3, 9\}$ . Lastly, we fix fluid and polymer viscosities such that  $\mu_s / (\mu_s + \mu_p) = 0.9$ .

We solve the fluid velocity and polymer conformation tensor field given by Eqs. (2.1a) and (2.1b) on a staggered, uniform, Cartesian grid, using the in-house flow solver [Fujin](#),

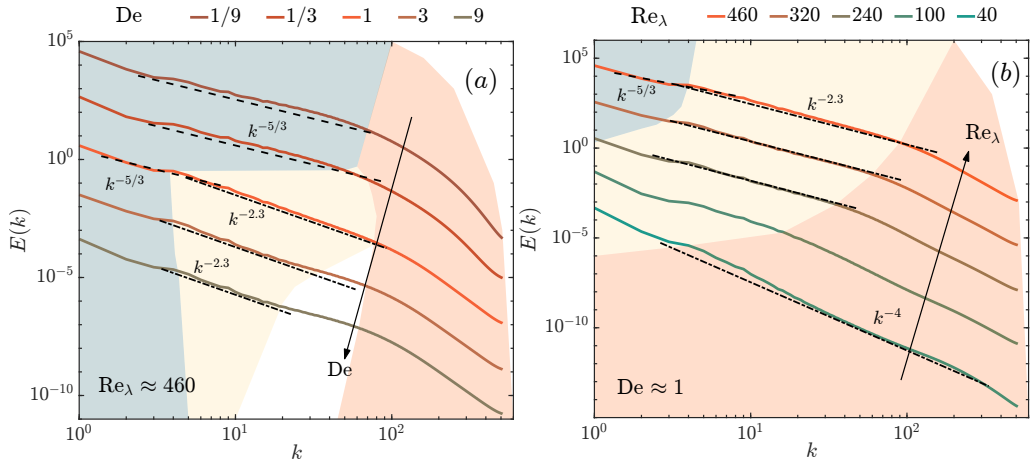


Figure 2: Multiscaling of the fluid energy spectrum  $E(k)$  in polymeric flows at different (a)  $De$  and (b)  $Re$  numbers. Three distinct scaling regimes (in different shades) have been shown in dashed ( $k^{-5/3}$ , Newtonian), dash-dotted ( $k^{-2.3}$ , polymeric) and dotted ( $k^{-\gamma}$ ;  $\gamma \geq 4$ , smooth) lines. All three regimes coexist when  $De \approx 1$ . (a) The smallest  $De$  has a close to Newtonian behaviour as the elastic effects are minimal. (b) The triple scaling at largest  $Re$  gives way to a unique, smooth  $k^{-4}$  regime at the smallest  $Re_\lambda$ .

which employs a second-order central finite difference scheme for spatial discretisation. Time marching is achieved via a second-order Adams-Bashforth scheme coupled with a fractional step method (Kim & Moin 1985), except for the non-Newtonian stress term which is advanced in time via the Crank-Nicolson scheme. A log-conformation formulation, together with a high-order Weighted Essentially Non-Oscillatory (WENO) scheme (Sugiyama *et al.* 2011) for the advection term of Eq. (2.1b) ensures positive-definiteness of the conformation tensor at all times (see Izbassarov *et al.* (2018)). Obtaining incompressible fluid velocity at each time requires solving a Poisson equation for pressure, which is done using a solver based on Fast Fourier Transform (FFT). The solver is parallelized using the domain decomposition library `2decomp` and the MPI protocol.

We solve Eq. (2.1) on a  $2\pi \times 2\pi \times 2\pi$ -periodic domain that is discretized into  $N^3 = 1024^3$  points. The smallest spatial scales resolved are equal to  $0.05\eta$  and  $\eta$  for the smallest and largest  $Re_\lambda$  simulations. We choose two different time-steppings of  $\delta t = 1.25 \times 10^{-5}$  and  $\delta t = 2.5 \times 10^{-5}$  for small and large  $Re_\lambda$  simulations, which respectively equal  $1.5 \times 10^{-3}\tau_\eta$  and  $2 \times 10^{-3}\tau_\eta$ , where  $\tau_\eta$  is the Kolmogorov time-scale. Field data is saved every  $2 \times 10^4$  time steps in a stationary state for data analysis. We show representative, two-dimensional slices of the dissipation fields  $\epsilon_f$  for very large and small  $Re$  in Fig. 1.

### 3. Results

#### 3.1. The energy spectra

We begin our study by investigating how energy is distributed across scales in a statistically stationary state in flows of polymeric fluids. The distribution of energy is given by its spectrum  $E(k)$  which is a measure of the energy content at scale (mode)  $k$  such that the total energy  $\mathcal{E} = \langle |\mathbf{u}|^2 \rangle / 2 = \int E(k) dk$ . Energy spectrum is one of the most commonly studied quantities in turbulence and was shown by Kolmogorov (1941) to have a self-similar distribution across scales in (the inertial range of) HIT as  $E(k) \sim k^{-5/3}$  (see also Frisch (1996)). We now show in Fig. 2 how this self-similar distribution of fluid kinetic energy is modified in PHIT, and

its dependence on polymer elasticity  $De$  in panel (a) and the intensity of turbulence  $Re_\lambda$  in panel (b).

Fig. 2(a) shows how the spectrum  $E(k)$  changes with  $De$  at large  $Re_\lambda \approx 460$ . When  $De$  is small, i.e. in the limit  $\tau_p \rightarrow 0$ , polymers are stiff, stretch minimally, and remain close to their equilibrium unstretched configuration  $\mathbf{C} \approx \mathbf{I}$ . This is easily seen by multiplying Eq. (2.1b) by  $\tau_p$ , and taking the limit  $\tau_p \rightarrow 0$ :

$$\tau_p (\partial_t \mathbf{C} + \mathbf{u} \cdot \nabla \mathbf{C}) = \tau_p (\mathbf{C} \nabla \mathbf{u} + (\nabla \mathbf{u})^T \mathbf{C}) - (\mathbf{C} - \mathbf{I}) \xrightarrow{\tau_p \rightarrow 0} \mathbf{C} - \mathbf{I} = 0. \quad (3.1)$$

As the fluctuations in  $\mathbf{C}$  are small, the polymer stresses in Eq. (2.1a) have a minimal contribution:  $\nabla \cdot \mathbf{C} \approx 0$ . Thus, elastic effects do not play a significant role at small  $De$ , and the behaviour remains largely Newtonian. This results in the classical K41, Newtonian like scaling  $E(k) \sim k^{-5/3}$  in Fig. 2(a). (Henceforth, we refer to this classical scaling range as the *Newtonian* regime.) This intermediate, *Newtonian* scaling range is of course followed by the dissipation range where the spectrum shows an exponential decay, a consequence of velocity fields being analytic.

As  $De$  is increased, polymers begin to stretch to longer lengths so that  $\mathbf{C}$  now ventures far from  $\mathbf{I}$  and has rather large spatio-temporal fluctuations. The resulting stretching and relaxation of polymers generates large non-Newtonian stresses (given by  $(\mu_p/\tau_p) \nabla \cdot \mathbf{C}$ ) on the carrier fluid, especially for a large enough elasticity as  $De \approx 1$ . The resulting dominant elastic effects alongwith a suppressed fluid non-linearity (see Section 3.2 for detailed discussion) means that the energy spectrum is modified to  $E(k) \sim k^{-2.3}$  at large  $Re_\lambda$ , as was also observed by Zhang *et al.* (2021a) and Rosti *et al.* (2023). (We refer to this as the *polymeric* range henceforth.) Viscous effects begin to dominate beyond this *polymeric* range and the fluid non-linearity ceases to have any contribution. The polymeric stresses, however, are still active in this range due to the small scale fluctuations in polymer lengths which, in turn, create fluctuations in the fluid velocity. Consequently, the spectrum exhibits a steep power-law decay  $E(k) \sim k^{-\delta}$  with  $\delta \geq 4$ , rather than an exponential fall-off in the smooth dissipative range. Thus, the elasticity of polymers results in a dual scaling behaviour of the energy spectrum  $E(k) \sim k^{-\delta}$  in PHIT, especially for  $De \approx 1$  (see Fig. 2(a)), with the exponent  $\delta \approx 2.3$  in the intermediate, polymeric range of scales ( $6 \lesssim k \lesssim 60$ ) and  $\delta \gtrsim 4$  for  $k \gtrsim 100$  in the smooth but steep dissipative .

On a further increase in polymer elasticity, the back reaction of polymers on the Newtonian carrier flow begins to diminish. This is because polymers with very large relaxation times respond to the background flow after a large time lag, thereby staying in a stretched configuration for long times. This means fluctuations in polymer lengths are suppressed at large  $De$ , thereby weakening the elastic stresses  $\nabla \cdot \mathbf{C}$  on an average. This is coupled with the fact that a large factor of  $\tau_p$  further weakens the feedback of polymer stresses on the carrier flow. Thus, *Newtonian* scaling is recovered for large  $De$ , and is seen in the re-emergence of  $E(k) \sim k^{-5/3}$  regime at  $De \approx 9$ . Indeed, at even larger  $De$  we have an intermediate range of scales with completely *Newtonian* scaling behaviour Rosti *et al.* (2023). Again in the deep dissipation range, small fluctuations in the polymer lengths result in fluctuations of the flow field, which are rough at the sub-leading order with a steep power-law decay of the spectrum as  $E(k) \sim k^{-4}$ .

Fig. 2(b) shows the dependence of the energy spectrum on  $Re_\lambda$ , where we plot  $E(k)$  for a fixed polymer elasticity of  $De \approx 1$ . The top curve is just the spectrum at  $Re_\lambda \approx 460$  and  $De \approx 1$ . Now, it is well known that with decreasing  $Re_\lambda$  in HIT the fluid non-linearity becomes increasingly less important (with respect to viscous dissipation) causing the inertial range to shrink (and the viscous dissipation range to widen). In PHIT, a decreasing  $Re_\lambda$  entails that now the intermediate *polymeric* range shrinks as seen from Fig. 2(b). This

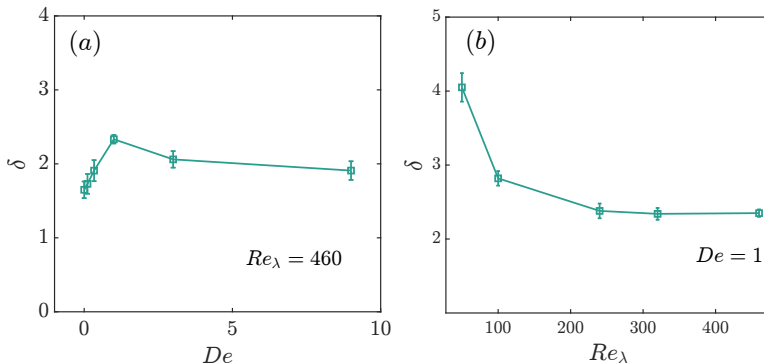


Figure 3: The dependence of the scaling exponent  $\delta$  for the fluid energy spectrum  $E(k) \sim k^{-\delta}$  on (a)  $De$  and (b)  $Re_\lambda$ . The exponents are computed for appropriate intermediate ranges, with the square markers showing the mean values, and the vertical lines indicating the error bars. (a) The presence of polymers leads to deviations from the K41 result of  $5/3$  (shown as  $De = 0$ ), especially at  $De \approx 1$  where  $\delta \approx 2.35$ . At very large  $De$ ,  $\delta \rightarrow 5/3$ . (b) The exponent  $\delta$  clearly saturates at large  $Re_\lambda$ , and the elastic turbulence regime is marked by  $\delta \approx 4$  as  $Re_\lambda \approx 40$ .

is a consequence of the fluid inertia weakening even further in the presence of polymers (see Section 3.2 for detailed discussion). A further weakened fluid inertia means that viscosity becomes important at even larger scales. The dissipative range thus widens, and the steep power-law fall-off begins at even smaller  $k$  as  $Re_\lambda$  decreases. In fact, at  $Re_\lambda \approx 40$ , the *polymeric* regime is completely absent and the smooth dissipation range spans the entire range of scales (see also Singh *et al.* (2024)). This is indeed very different from Newtonian turbulence, where a decreasing  $Re_\lambda$  results in a shrinking inertial range that completely disappears as  $Re_\lambda \rightarrow 0$  and the spectrum decays exponentially. Polymeric turbulence, on the other hand, shows a transition from  $E(k) \sim k^{-2.3}$ , as  $Re_\lambda$  decreases, to a steeper power-law spectrum of  $E(k) \sim k^{-4}$  as  $Re_\lambda \rightarrow 0$  for large  $De$ .

We close this section by plotting in Fig. 3 the spectrum exponent  $\delta$  for  $E(k) \sim k^{-\delta}$ . Panel (a) shows that  $\delta$  depends non-monotonically on  $De$  (at large  $Re_\lambda$ ), while it changes monotonically with  $Re_\lambda$  (for  $De = 1$ ) in panel (b). Next, we discuss how different dominant contributions lead to this multiscaling behaviour in polymeric flows, as a function of  $Re_\lambda$  and  $De$ .

### 3.2. The flux contributions

The co-existence of various scaling regimes of the energy spectrum, as discussed in Section 3.1, can be better understood by looking at the dominant energy transfer mechanisms across scales. We obtain these dominant contributions from Eq. (2.1a) by computing its Fourier transform and its complex conjugate,

$$\partial_t \hat{u}_i(\mathbf{k}) + \mathcal{N}_i(\mathbf{k}) = ik_i \hat{p} - \nu k^2 \hat{u}_i(\mathbf{k}) + \frac{\mu_p}{\rho \tau_p} ik_j \hat{C}_{ij} + \hat{F}_i(\mathbf{k}), \quad k_i \hat{u}_i = 0; \quad (3.2a)$$

$$\partial_t \hat{u}_i^\dagger(\mathbf{k}) + \mathcal{N}_i^\dagger(\mathbf{k}) = -ik_i \hat{p}^\dagger - \nu k^2 \hat{u}_i^\dagger(\mathbf{k}) - \frac{\mu_p}{\rho \tau_p} ik_j \hat{C}_{ij}^\dagger + \hat{F}_i^\dagger(\mathbf{k}), \quad (3.2b)$$

where the hat  $\hat{\cdot}$  denotes the Fourier transformed variables,  $\cdot^\dagger$  denotes the complex conjugate, and  $\mathcal{N}_i(\mathbf{k})$  is the Fourier transform of the fluid non-linear term. Summation over repeated indices is implied. The energy equation for any  $k$ -th mode can be obtained by multiply-

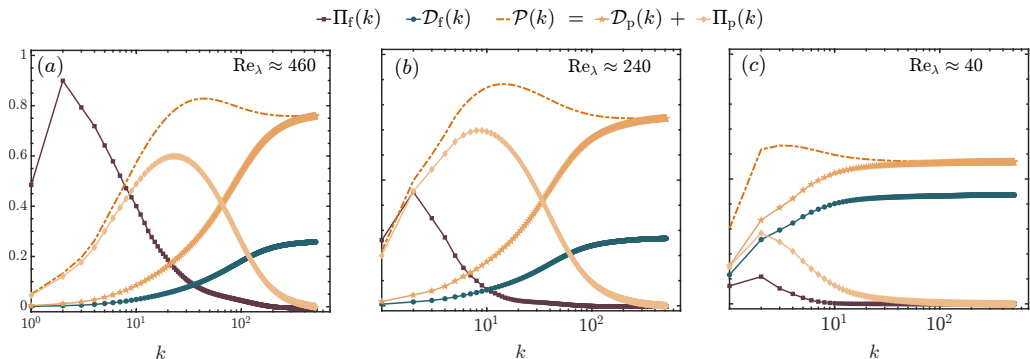


Figure 4: Normalized flux contributions at (a)  $Re_\lambda \approx 460$ , (b) 240, and (c) 40 for flows with  $De \approx 1$ . (a) At large  $Re_\lambda$ , three distinct regimes are determined by different dominant contributions: large scales are dominated by the fluid non-linear flux  $\Pi_f$ , intermediate scales by the polymer flux  $\Pi_p$ , and small scales by the polymer dissipation  $\mathcal{D}_p$ . (b) At moderate  $Re_\lambda$ , the fluid-nonlinearity  $\Pi_f$  is weakened and comprises two distinct regimes dominated by  $\Pi_p$  and  $\mathcal{D}_p$ . (c) At extremely small  $Re_\lambda$ , only the dissipative terms  $\mathcal{D}_f$ ,  $\mathcal{D}_p$  remain important.

ing Eq. (3.2a) by  $u_i^\dagger(\mathbf{k})$ , and Eq. (3.2b) by  $u_i(\mathbf{k})$ , and adding the two together:

$$\partial_t \mathcal{E}(\mathbf{k}) + \Re \left( \hat{u}_i^\dagger(\mathbf{k}) \mathcal{N}_i(\mathbf{k}) \right) = -2\nu k^2 \mathcal{E}(\mathbf{k}) + \frac{\mu_p}{\rho \tau_p} \Im \left( \hat{u}_i^\dagger(\mathbf{k}) k_j \hat{C}_{ij} \right) + \Re \left( \hat{u}_i^\dagger(\mathbf{k}) \hat{F}_i(\mathbf{k}) \right), \quad (3.3)$$

where  $\mathcal{E}(\mathbf{k}) = |\hat{u}_i(\mathbf{k})|^2/2$  is the energy in mode  $\mathbf{k}$ , the pressure term vanishes away due to incompressibility, and  $\Re(\cdot)$  and  $\Im(\cdot)$  denote the real and imaginary parts respectively. The total energy flux from modes  $k < K$  to those  $k > K$  can be obtained by integrating from 0 to  $K$ :

$$\begin{aligned} \partial_t \int_0^K d\mathbf{k} \mathcal{E}(\mathbf{k}) + \int_0^K d\mathbf{k} \Re \left( \hat{u}_i^\dagger(\mathbf{k}) \mathcal{N}_i(\mathbf{k}) \right) = \\ -\nu \int_0^K d\mathbf{k} k^2 |\hat{u}_i(\mathbf{k})|^2 + \frac{\mu_p}{\rho \tau_p} \int_0^K d\mathbf{k} \Im \left( \hat{u}_i^\dagger(\mathbf{k}) k_j \hat{C}_{ij} \right) + \int_0^K d\mathbf{k} \Re \left( \hat{u}_i^\dagger(\mathbf{k}) \hat{F}_i(\mathbf{k}) \right). \end{aligned} \quad (3.4)$$

In a statistically stationary state, the total energy in any set of modes is a constant, so that  $\partial_t \int_0^K d\mathbf{k} \mathcal{E}(\mathbf{k}) = 0$ . Choosing suitable symbols for the remaining integrals, and using isotropy to argue that their dependence is only on  $K = |\mathbf{K}|$ , we have:

$$\Pi'_f(K) = -\mathcal{D}'_f(K) - \mathcal{P}'(K) + \mathcal{F}(K), \quad (3.5)$$

where  $\Pi'_f$ ,  $\mathcal{D}'_f$ ,  $\mathcal{P}'$ , and  $\mathcal{F}$  are the contributions from fluid non-linearity, fluid dissipation, polymer stresses, and the external forcing, respectively. Since the forcing  $\hat{F}_i$  is applied at only  $K = 1$ , we have that  $\mathcal{F}(K)$  is a constant for any  $K > 1$ :

$$\Pi'_f(K) + \mathcal{D}'_f(K) + \mathcal{P}'(K) = \mathcal{F}(K) = \epsilon_t, \quad (3.6)$$

where  $\epsilon_t$  is the rate of total energy injection into the system by the forcing  $\mathbf{F}$ . Thus, upon normalization by  $\epsilon_t$ , we obtain:

$$\Pi_f(K) + \mathcal{D}_f(K) + \mathcal{P}(K) = 1, \quad (3.7)$$

where  $\Pi_f = \Pi_f'/\epsilon_t$ ,  $\mathcal{D}_f = \mathcal{D}_f'/\epsilon_t$ ,  $\mathcal{P} = \mathcal{P}'/\epsilon_t$ . We show the curves for all the three contributions,  $\Pi_f$ ,  $\mathcal{D}_f$ , and  $\mathcal{P}$ , as a function of  $Re_\lambda$  in Fig. 4, for a polymer elasticity of  $De \approx 1$ . Following Rosti *et al.* (2023), we partition the polymeric contribution into flux ( $\Pi_p$ ) and dissipative ( $\mathcal{D}_p$ ) terms as:

$$\mathcal{P}(K) = \Pi_p(K) + \mathcal{D}_p(K), \quad \text{where} \quad \mathcal{D}_p(K) \equiv (\epsilon_p/\epsilon_t)\mathcal{D}_f(K). \quad (3.8)$$

Such a definition is motivated by the requirement that at small scales (or large  $k$ ) the polymeric term must get all its contribution from dissipative effects. However, this choice of  $\mathcal{D}_p$  is not unique reasonable alternative definitions do not affect the qualitative conclusions. We also plot the contributions  $\Pi_p$  and  $\mathcal{D}_p$  thus obtained in Fig. 4.

At large  $Re_\lambda$ , Fig. 4(a) shows that the fluid non-linearity  $\Pi_f$  has the dominant contribution to the total energy balance at large scales (i.e. for  $k \leq 4$ ). This gives the *Newtonian*  $k^{-5/3}$  scaling at the large but slim band of scales in Fig. 2. Away from this range, i.e. for  $k \geq 10$ , the polymeric flux contribution  $\Pi_p$  begins to dominate. This dominant non-Newtonian flux results in a *polymeric* scaling regime with  $E(k) \sim k^{-2.3}$  upto  $k \approx 70$  in Fig. 2 (see also Rosti *et al.* (2023)). At yet smaller scales, i.e. for  $k \geq 200$ , fluid ( $\mathcal{D}_f$ ) and polymer ( $\mathcal{D}_p$ ) dissipation remove energy from the flow rapidly. The polymer contribution  $\Pi_p$ , has a small, sub-dominant yet non-zero contribution in this range. (This aligns with our assertion of small scale fluctuations in polymer lengths in Section 3.1.) This sub-dominant contribution results in a fluid velocity spectrum given by a steep power-law decay at large  $k$ , in a manner similar to that in ET at very small  $Re_\lambda$  (see Singh *et al.* (2024)). Now, as  $Re_\lambda$  is decreased to a moderate value of  $Re_\lambda \approx 240$ , the fluid non-linearity is weakened evidently further as seen in Fig. 4(b), and the flux of energy is primarily via the fluid-polymer interactions  $\Pi_p$ . However, this range is rather limited as a smaller  $Re_\lambda$  also means that viscous effects become important at relatively smaller  $k$ . Thus, we have a restricted *polymeric* and a wider  $k^{-4}$  regime at  $Re_\lambda \approx 240$  in Fig. 2(b). Finally, for very small  $Re_\lambda \approx 40$  in Fig. 4(c),  $\mathcal{D}_p$  and  $\mathcal{D}_f$  are always large while  $\Pi_f$  and  $\Pi_p$  remain sub-dominant. In fact,  $\Pi_f$  at such small  $Re_\lambda$  is expected to be dormant and indeed shows an exponential fall off in wave-numbers  $k$  in Fig. 5(c).  $\Pi_p$  instead decays only as a steep power-law, and forces fluctuations in the velocity field that result in the steep, and extended  $k^{-4}$  range in Fig. 2(d).

### 3.3. Slowing down the energy cascade

While the above discussion in Section 3.1 on flux contributions sheds light on the multiscaling nature of the energy spectra, there is more that remains in hiding in Fig. 4. We uncover this by plotting the flux contributions on a log-log scale in Fig. 5 which clearly reveals the  $k$ -dependence of the flux contributions. We are particularly interested in the fluid  $\Pi_f$  and polymeric  $\Pi_p$  fluxes.

Fig. 5(a) shows that at large  $Re_\lambda$  our *polymeric* regime  $E(k) \sim k^{-2.3}$  is marked by a fluid non-linear flux decaying as  $\Pi_f \sim k^{-1.2}$ , while  $\Pi_p$  remains almost constant. Now,  $E(k)$  and  $\Pi_f$  can be related to each other using the following simple arguments.  $\Pi_f$  is the average rate of net energy transfer through a scale  $k$ . This means velocity fluctuations  $u_k$ , at scale  $k$ , transfer their energy to smaller scales in some characteristic time  $\tau_k \sim (ku_k)^{-1}$ . In HIT, this characteristic time-scale is equal to the typical lifetime of an eddy within the K41 phenomenology. This is because energy flux  $\Pi_{f,N}$  in the inertial range is a constant, i.e.  $\Pi_{f,N} = \epsilon$ , with  $\epsilon$  being the average rate of energy dissipation. Therefore, we have

$$\Pi_{f,N} \sim \frac{u_k^2}{\tau_k} \sim ku_k^3 \sim \epsilon \implies u_k \sim k^{-1/3} \quad (3.9)$$

in the inertial range of scales. This means that the time to transfer energy to smaller scales

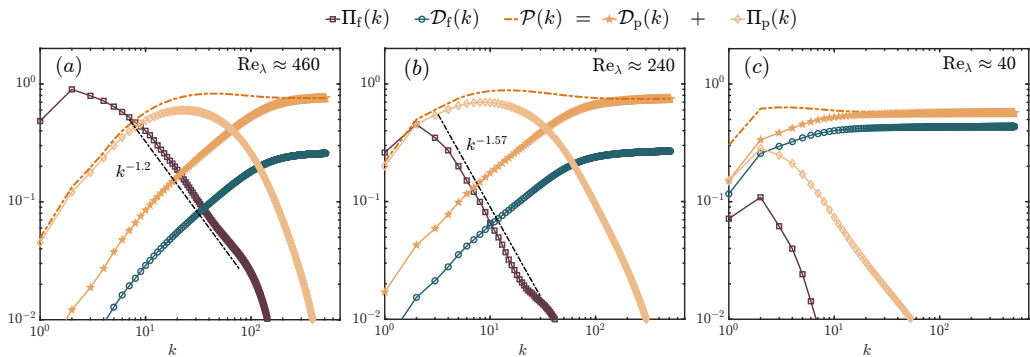


Figure 5: The scaling behaviour of flux contributions obtained by replotting Fig. 4 on a log-log scale. The approximate scaling forms are shown as dash-dotted lines. The fluid flux  $\Pi_f$  decays as a power-law in the presence of polymers at large to moderate  $Re_\lambda$ , implying a slow and weak fluid non-linear cascade.

and the typical lifetime of eddies are respectively estimated as

$$\tau_{k,N} \sim \frac{u_k^2}{\Pi_{f,N}} \sim \frac{kE_k}{k^0} \sim k^{-2/3} ; \quad \tau_{k,N} \sim (ku_k)^{-1} \sim (kk^{-1/3})^{-1} \sim k^{-2/3}. \quad (3.10)$$

In HIT, these time scales are identical as they both are a consequence of a constant inertial range energy flux  $\Pi_{f,N}$ . This, however, is no longer true in PHIT where the fluid non-linear flux  $\Pi_f$  is no longer a constant, but is rather a function of the scale  $k$  (and therefore is no longer the invariant that determines the scaling form of the velocity fluctuations). This means we have two different estimates for the scale-by-scale energy transfer rate and the typical lifetimes (of  $u_k$ ) in PHIT. Using data from numerical simulations plotted in Fig. 3 and Fig. 5(a) we obtain

$$\tau_k \sim \frac{u_k^2}{\Pi_f} \sim \frac{kE_k}{k^{-1.2}} \sim k^{-0.15} ; \quad \tau_k \sim (ku_k)^{-1} \sim \left(k\sqrt{kE_k}\right)^{-1} \sim k^{-0.325}. \quad (3.11)$$

The first estimate gives the rate at which energy is transferred to smaller scales via the non-linear cascade process while the second estimate gives the typical lifetime of fluctuations. The two suggest that, on an average, velocity fluctuations in PHIT die faster than they transfer energy to smaller scales. This is indeed possible now as energy is also transferred to polymers so that the typical lifetime of the fluctuations is determined by the average rates of the two energy transfer processes, i.e. fluxes. Indeed, a crude assumption using Fig. 5(a) of  $\mathcal{P} \approx \text{constant}$  in the range where  $\Pi_f \sim k^{-1.2}$ , we obtain the rate at which energy is lost to the polymeric mode as

$$\tau_k \sim \frac{u_k^2}{\Pi_p} \sim \frac{kE_k}{k^0} \sim k^{-1.35}. \quad (3.12)$$

Two observations are immediate. First, the rate of energy transfer to the polymeric mode is much faster than that to smaller scales of the fluid itself. Second, the typical lifetime of the fluctuations  $\tau_k \sim k^{-0.325}$  (see Eq. (3.11)) lies somewhere between the time scales determined by the two fluxes ( $k^{-0.15}$  and  $k^{-1.35}$ ). Thus, the addition of polymers has the effect of slowing down the cascade process while the rate of energy transfer to polymeric mode is much faster. Additionally, this slower cascade, along with a smaller scale-by-scale energy given by  $E(k) \sim k^{-2.3}$  means that the velocity fluctuations take much longer to transfer energy to

smaller scales in PHIT (compared to HIT), thus resulting in a slower as well as a weaker cascade in PHIT.

At smaller  $Re_\lambda$ , the cascade process is weakened even further as smaller scales take even longer to transfer energy via the cascade process. This is again seen via the respective estimates at  $Re_\lambda \approx 240$ :

$$\tau_k \sim \frac{u_k^2}{\Pi_f} \sim k^{0.22}; \quad \tau_k \sim (ku_k)^{-1} \sim k^{-0.325}; \quad \tau_k \sim \frac{u_k^2}{\Pi_p} \sim \frac{kE_k}{k^0} \sim k^{-1.35}. \quad (3.13)$$

where we have used  $u_k^2 \sim kE_k \sim k^{-1.35}$  (Fig. 3(b)) and  $\Pi_f \sim k^{-1.57}$  (Fig. 5). Clearly, the cascade process is even more weakened while energy is being transferred to the polymeric mode even faster. Again, as a check, the lifetime of fluctuations (middle) lies in between the two transfer rates (left and right). At the smallest  $Re_\lambda \approx 40$  in Fig. 5(c), the non-linear term falls-off exponentially in  $k$ , which means there is practically no energy transfer via the cascade process. This is not surprising as the non-linear term is expected to be inactive at such small  $Re_\lambda$ .

In a nutshell, the effect of the addition of polymers is to slow down the cascade process which we quantify using scaling arguments the knowledge of flux contributions, and the fluid energy spectra. In the next section, we discuss how energy is distributed in the polymeric scales of motion via the polymer energy spectrum using data as well as scaling arguments.

### 3.4. The polymer spectra

The distribution of energy across polymeric scales, in a statistically stationary state, can be obtained by computing the polymer energy spectrum  $E_p(k)$  in analogy with the fluid energy spectrum  $E(k)$ . To do so, we start by defining the polymer energy spectrum in a sense similar to that of [Balci et al. \(2011\)](#) and [Nguyen et al. \(2016\)](#). The measure of average total polymer energy  $\mathcal{E}_p$  is given by the  $\text{Tr}[\mathbf{C}]$  as (see also [Balci et al. \(2011\)](#))

$$\mathcal{E}_p = \frac{\mu_p}{2\tau_p} \langle \text{Tr}[\mathbf{C}] \rangle = \frac{\mu_p}{2\tau_p V} \int_V C_{ii}(\mathbf{x}) d\mathbf{x} = \frac{\mu_p}{2\tau_p V} \int_V B_{ij}(\mathbf{x}) B_{ji}(\mathbf{x}) d\mathbf{x}, \quad (3.14)$$

where  $\mathbf{B}$  (with components  $B_{ij}$ ) is the positive-definite square root of the conformation tensor  $\mathbf{C}$ , i.e.  $C_{ij}(\mathbf{x}, t) = B_{ik}(\mathbf{x}, t) B_{kj}(\mathbf{x}, t)$ . One can now define the polymer energy spectrum  $E_p(k)$  by employing Parseval's relation

$$\begin{aligned} \mathcal{E}_p &= \frac{\mu_p}{2\tau_p V} \int_V B_{ij}(\mathbf{x}) B_{ji}(\mathbf{x}) d\mathbf{x} = \frac{\mu_p}{2\tau_p V} \int_{\mathbb{R}^3} B_{ij}(\mathbf{k}) B_{ji}(-\mathbf{k}) d\mathbf{k} = \int_0^\infty E_p(k) dk \\ &\quad \text{where } E_p(k) = \frac{\mu_p}{2\tau_p V} \int_{|\mathbf{k}|=k} B_{ij}(\mathbf{k}) B_{ji}(-\mathbf{k}) d\Omega_k, \end{aligned} \quad (3.15)$$

where  $V$  is volume of integration and the last integral is defined over a spherical shell of radius  $k$ .

Now, the scale-by-scale energy  $(\mu_p/2\tau_p)C_k$  can then be estimated as the energy contained in the modes  $\in [k, k + dk]$ :

$$\frac{\mu_p}{2\tau_p} C_k = E_p(k) dk, \quad (3.16)$$

in analogy with the classical

$$\frac{1}{2} u_k^2 = E_k(k) dk. \quad (3.17)$$

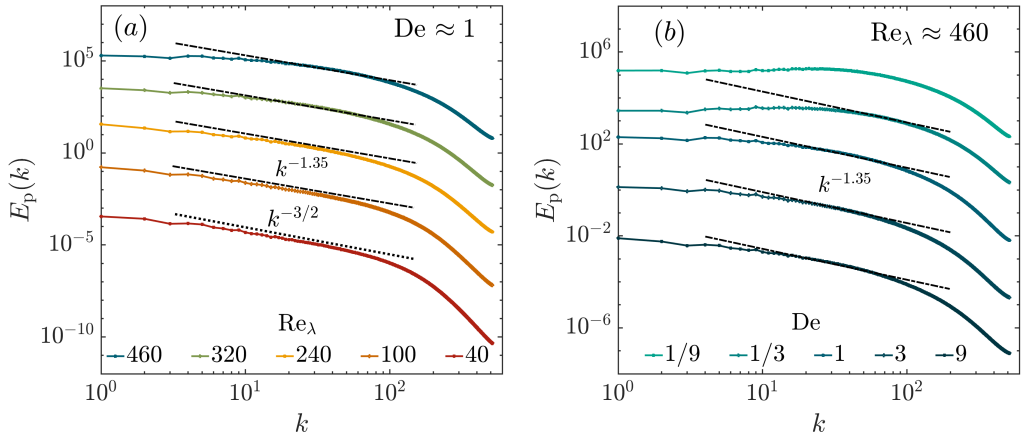


Figure 6: The dependence of the polymer energy spectrum  $E_p(k)$  on (a)  $Re_\lambda$  (shown for  $De \approx 1$ ), and on (b)  $De$  (shown for  $Re_\lambda \approx 460$ ). The two different scaling regimes with exponents  $-1.35$  (at large  $Re$ ) and  $-1.5$  (at small  $Re$ ) are shown in dash-dotted and dotted lines, respectively. (b) Small  $De$  flows at large  $Re$  show a close to Newtonian behaviour and  $E_p(k)$  remains devoid of any scaling form. As  $De \gtrsim 1$ , the expected scaling with exponent  $-1.35$  begins to appear.

Thus, it is easy to see using dimensional arguments that  $C_k \sim kE_p(k)$ , similar to  $u_k^2 \sim kE_k(k)$ . We now use this relation to estimate  $E_p(k)$  by relating it with  $E(k)$ .

Let us begin by looking at the  $\Pi_p$  curves in Fig. 4 (or Fig. 5). For large  $Re_\lambda$ , the flux contribution  $\Pi_p$  remains approximately constant for  $k \in [20, 60]$ . Therefore,

$$\frac{\mu_p}{\tau_p} k u_k C_k \sim k^0 \implies C_k \sim (k u_k)^{-1} \sim k^{-0.35}. \quad (3.18)$$

This immediately implies, using Eq. (3.16), that  $E_p(k) \sim k^{-1} C_k \sim k^{-1.35}$  for  $k \in [20, 60]$ . Indeed, we find this to be consistent with the data from simulations plotted in Fig. 6(a). At  $Re_\lambda \approx 240$ , this scaling range of  $E_p(k)$  shows a slight shift to larger scales, in correspondence to a similar shift of constant  $\Pi_p$  in Fig. 5. At the smallest  $Re_\lambda \approx 40$ , however, dissipative effects become dominant so that polymeric contribution  $\mathcal{P}$  to the total flux is of the same order as  $\mathcal{D}_f$  for  $k \gtrsim 10$  in Fig. 5(c). Hence, a simple comparison of the fluid dissipation and polymer terms gives (see also Singh *et al.* (2024))

$$k^2 u_k \sim k C_k \implies E_p(k) \sim u_k \sim \sqrt{k E_k} \sim k^{-3/2}, \quad (3.19)$$

which is also consistent with the data shown in Fig. 6(a).

We show the variation with  $De$  of the polymer spectrum in Fig. 6(b) for large  $Re_\lambda$ . At very small  $De$ , the polymers barely stretch so that their lengths remain almost constant (with rather small fluctuations), implying an approximately flat spectrum over a significant range of scales. At small scales, the fields must be analytic as a result of which the spectrum at large  $k$  falls-off exponentially. As the polymers stretch more with increasing  $De$ , fluctuations over a wide range of scales begin to appear. The scale dependence of the fluctuations is then given by  $E_p(k)$  discussed above. The cleanest scaling range appears when elasticity is large, when the polymers extend to larger lengths and provide a self-similar distribution of polymer energy over a wide range of scales.

We now move on to real space statistics, by first discussing the multiscaling nature using structure functions, complementing the discussion in Section 3.1.

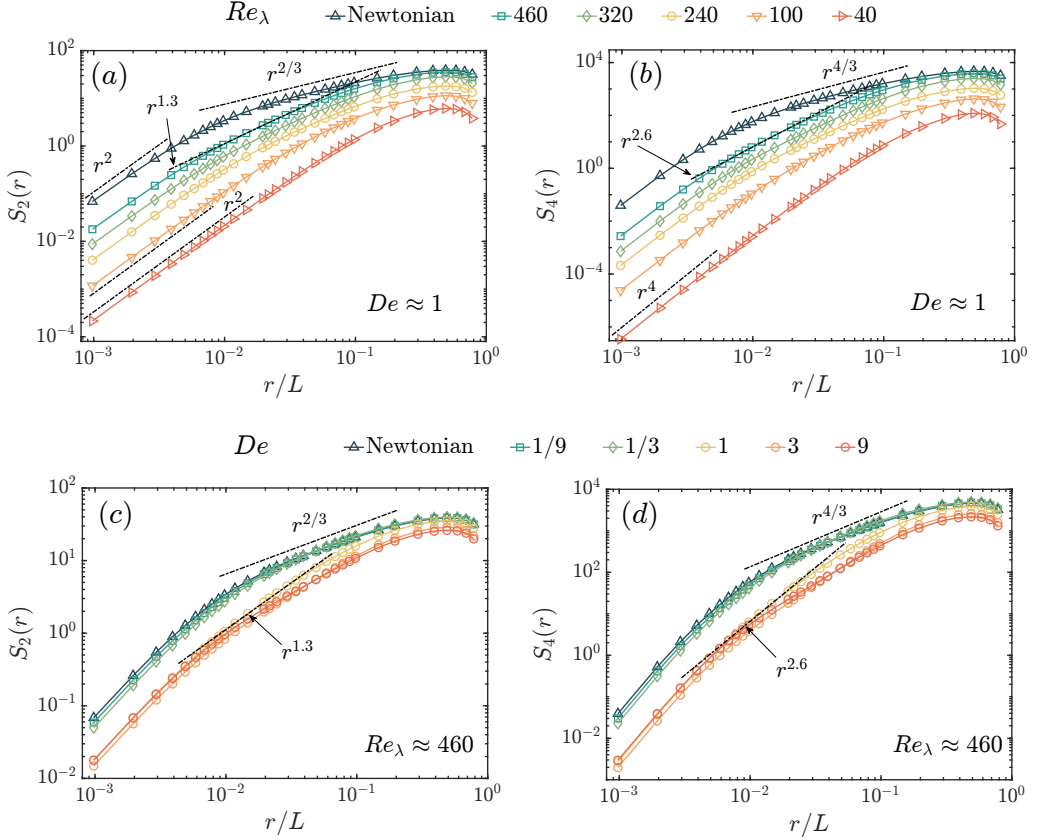


Figure 7: Manifestation of the multiscaling behaviour in the structure functions of second ( $S_2$ : panels a,c) and fourth ( $S_4$ : panels b,d) orders. (Top) Panels (a,b) show the dependence on  $Re_\lambda$ , while (Bottom) panels (c,d) show the dependence on the polymer elasticity  $De$ . Note that the (c)  $S_2(r)$  and (d)  $S_4(r)$  curves fall on top of the Newtonian for small  $De$ . At large  $De$ , the elastic scaling regime becomes clear as elasticity begins to play a significant role showing a clear departure from the Newtonian curve.

### 3.5. Velocity differences and structure functions

In this section, we discuss how a multiscaling behaviour is also manifested in the real-space statistics of PHIT. This complements the Fourier space discussion of Section 3.1. One of the most common real-space measures that admit a scaling behaviour in turbulence are the well known structure functions  $S_p(r)$ , defined as the  $p$ -th moments of the longitudinal velocity increments  $\delta_r u$  over a separation  $r$ :

$$\delta_r u \equiv [\mathbf{u}(\mathbf{x} + \mathbf{r}) - \mathbf{u}(\mathbf{x})] \cdot \hat{\mathbf{r}}, \quad (3.20)$$

$$S_p(r) = \langle (\delta_r u)^p \rangle = \frac{1}{3} \sum_{i=1}^3 \langle [u_i(x_i + r_i) - u_i(x_i)]^p \rangle. \quad (3.21)$$

In particular,  $S_2(r)$  is related to the energy spectrum  $E(k)$  via a Fourier transform (see Frisch (1996))

$$S_2(r) = \frac{1}{2\pi} \int E(k) e^{-ikr} dk. \quad (3.22)$$

One can then easily use the above to relate the power-law behaviour of  $S_2$  and  $E(k)$ . Consider that the separation in the real-space  $r$  is scaled by a factor  $b$ ,  $r \rightarrow br$ , so that the Fourier space wave number scales as  $k \rightarrow b^{-1}k$ . Consequently, if the spectrum scales with an exponent  $\alpha$ , i.e.  $E(k) \sim k^{-\alpha}$ , then  $E(k) \rightarrow E(bk) = b^{-\alpha}E(k)$ . Therefore, Eq. (3.22) can be rewritten under the rescaling as:

$$S_2(br) = \frac{1}{2\pi} \int dk E(k) e^{-ikbr} = \frac{1}{2\pi} \int (b^{-1}dk) (b^\alpha E(k)) e^{-ikr} = b^{\alpha-1} S_2(r). \quad (3.23)$$

Hence, we have that  $E(k) \sim k^{-\alpha} \iff S_2(r) \sim r^{\alpha-1}$ . Note that this relation holds only for  $\alpha \leq 3$ . For  $\alpha > 3$ , the real-space exponent is given via the leading order in Taylor expansion as  $S_2 \sim r^2$ . In HIT, these arguments imply that  $S_2 \sim r^{2/3}$  given  $E(k) \sim k^{-5/3}$  whereas in PHIT we now expect  $S_2 \sim r^{1.3}$  using  $E(k) \sim k^{-2.3}$ . Additionally, using dimensional arguments, one also expects within the K41 phenomenology that  $S_4 \sim S_2^2$ . With these expected results in mind, we show in Fig. 7(a,b) the plots of  $S_2(r)$ ,  $S_4(r)$  for PHIT at different  $Re_\lambda$  and  $De \approx 1$  alongside the HIT result. The variation of  $S_2(r)$  and  $S_4(r)$  with  $De$  is shown in Fig. 7(c,d). We of course have that the HIT structure functions follow the Kolmogorov scaling  $r^{p/3}$  closely in Fig. 7(a,b), while those for PHIT show a very clear departure from this behaviour. Indeed, and in consistency with the discussion above, the *polymeric* scaling is given by  $S_2 \sim r^{1.3}$  ( $S_4 \sim r^{2.6}$ ) and is seen to have the widest span at the largest  $Re_\lambda \approx 460$ . This is also consistent with the discussion in Section 3.1 where we show that the *polymeric* regime shrinks with decreasing  $Re_\lambda$ , while the smooth dissipation range marked by  $S_2 \sim r^2$  expands (corresponding to  $E(k) \sim k^{-4}$  in Fig. 2). At the smallest  $Re_\lambda \approx 40$ , the smooth scaling  $S_2 \sim r^2$  spans almost a decade.

We show the variation of the structure functions with  $De$  in Fig. 7(c,d). As expected from Fig. 3(a), this dependence is rather non-monotonic. The small  $De$  cases show an approximately Newtonian behaviour, owing to the minimal non-Newtonian contributions as the polymers strongly resist any stretching (see Section 3.1 for detailed discussion). As  $De \rightarrow 1$ , we have a clear *polymeric* scaling  $S_2 \sim r^{1.3}$  ( $S_4 \sim r^{2.6}$ ). This steeper than Kolmogorov slope starts to vanish when polymer elasticity is further increased, and the  $S_2/S_4$  curves now have a shallower slope. At much larger polymer elasticity one indeed recovers the Kolmogorov scaling (see Rosti *et al.* (2023)). This behaviour is again in consistency with that for the spectrum in Section 3.1.

We also make an important note about Fig. 7(b,d). The  $S_4(r)$  curves evidently show smaller scaling ranges compared to those of  $S_2(r)$  in Fig. 7(a,c). This means that the exponents quickly deviate from the naive expectation of  $S_4(r) \sim S_2^2(r)$ . This is not only an artefact of the deviations from a K41 like behaviour but also captures the non-Gaussianity of  $\delta_r u$ . We quantify these deviations by measuring the *kurtosis* of the velocity increment distributions in the next section.

### 3.6. Kurtosis of velocity differences

Consider the distribution of (longitudinal) velocity differences  $\delta_r u$ , defined by Eq. (3.20), as a function of the scale  $r$ . The kurtosis (or flatness)  $\mathcal{K}(r)$  of such a distribution is defined as:

$$\mathcal{K}(r) \equiv \frac{\langle (\delta_r u)^4 \rangle}{\langle (\delta_r u)^2 \rangle^2}. \quad (3.24)$$

The kurtosis  $\mathcal{K}$  captures the relative importance of the tails of a distribution and quantifies their contribution to the overall statistics of  $\delta_r u$ . For a Gaussian distribution,  $\mathcal{K} = 3$ . We expect the velocity increments to be uncorrelated over very large separations, so that the distribution of  $\delta_r u$  is close to a Gaussian for large  $r$ . This is indeed confirmed in our data

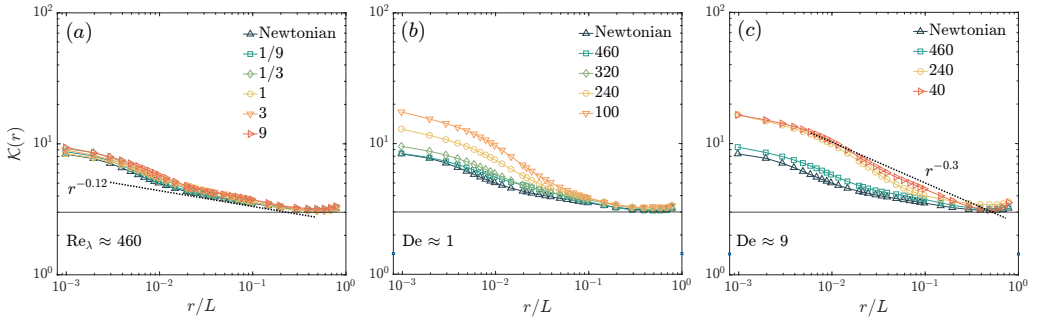


Figure 8: The kurtosis of velocity differences as a function of scale  $r$ .  $\mathcal{K} \rightarrow 3$  as  $r \rightarrow L$  as velocity differences decorrelate at very large separations. (a)  $\mathcal{K}$  at large  $Re_\lambda \approx 460$  and different  $De$  are almost coincident implying a very weak dependence of intermittency on  $De$ . (b,c) Intermittency in polymeric flows increases as  $Re_\lambda$  is decreased, especially when  $De$  is large.

in Fig. 8 where we find  $\mathcal{K}(r) \approx 3$  for large  $r$ , irrespective of  $Re_\lambda$  and  $De$ . More importantly,  $\mathcal{K}$  is not a constant but a function of the scale  $r$ . The distributions of  $\delta_r u$  are, evidently, devoid of scale-invariance and their departures from Gaussianity become increasingly stronger at small  $r$ . This is a result of more important contributions from the tails of the distribution of  $\delta_r u$ , a phenomenon referred to as intermittency, and causes deviations from the dimensional expectation of  $S_4 \sim S_2^2$  (this would have meant  $\mathcal{K} \sim r^0$  from Eq. (3.24)). The log-log plots of  $\mathcal{K}$  in Fig. 8(a) clearly show a power-law dependence on  $r$  at large  $Re_\lambda \approx 460$ . Crucially, this power-law is very weakly dependent on  $De$  as the curves for different  $De$  follow each-other closely. Thus, the intermittent nature of the velocity fluctuations is still largely determined by the fluid non-linearity. This was also observed by Rosti *et al.* (2023) via the multifractal spectrum for energy dissipation. The influence of polymers on velocity fluctuations, however, is more apparent at small  $Re_\lambda$ , as shown in Fig. 8(b). At small  $Re_\lambda$ , although the fluid non-linearity becomes considerably weaker (see Fig. 5(b)), the polymer stresses feeding back on the flow result in the velocity fluctuations  $\delta_r u$  being more intermittent, and the departure from HIT curve becomes significant. This is even more pronounced at the smallest  $Re_\lambda$  (we considered) where the presence of polymers results in much large deviations of  $\delta_r u$  at small  $r$  which is manifested in a much steeper slope of the kurtosis  $\mathcal{K}(r) \sim r^{-0.3}$  compared to the Newtonian.

So, the departure from a Kolmogorov-like behaviour in polymeric flows is not only due to a modified energy flux—resulting in a different scaling of the spectrum—but also due to the modified nature of extreme fluctuations that result from the action of the polymer stresses. This also underlines the fact that intermittency is due not only to fluid non-linearity but even polymer stresses can drive highly intermittent velocity fluctuations. Such intermittent behaviour is also discernible in the statistics of velocity gradients. In the following sections, we discuss the intermittent nature of velocity gradients, and how they influence the stretching of polymers. This also forms the basis for the discussion of the two energy dissipation rates: fluid  $\epsilon_f$  and polymer  $\epsilon_p$ .

### 3.7. Polymer stretching, velocity gradients, and their relation to the energy dissipation

We now discuss in this section how polymers of different  $De$  are themselves affected by the fluid flow at different  $Re_\lambda$ . To this end, we begin by simply looking at the stretching statistics of the polymers. measure of the stretching of the polymers is their end-to-end lengths whose instantaneous squared value is given by  $\text{Tr}[\mathbf{C}]$ . We naturally expect polymers to stretch more with increasing  $De$  at any given  $Re_\lambda$ . In the limit of  $De \rightarrow 0$ , it can be seen from Eq. (2.1b)

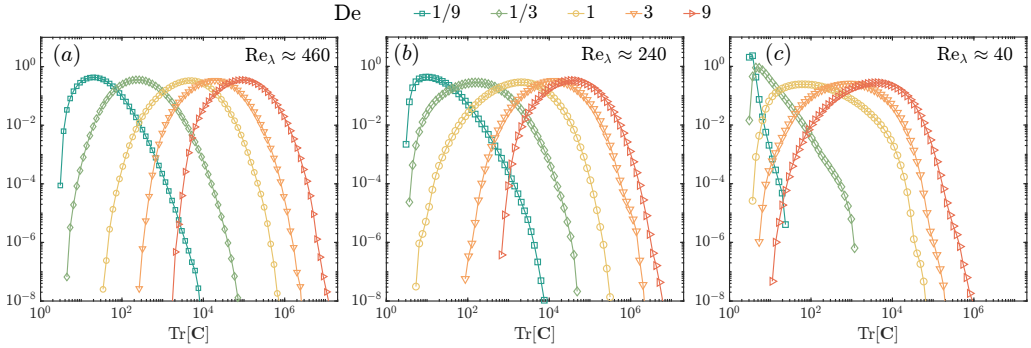


Figure 9: Pdfs of the end-to-end polymer lengths  $\text{Tr}[\mathbf{C}]$  for different  $Re_\lambda$ : (a)  $Re_\lambda \approx 460$ , (b)  $Re_\lambda \approx 240$ , and (c)  $Re_\lambda \approx 40$  and all  $De$ . A large  $De$  polymer has a larger average end-to-end length, as seen in the right shift of the pdfs.

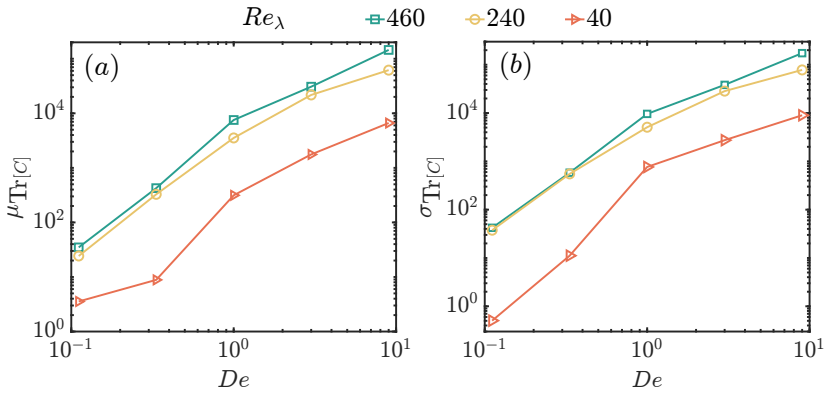


Figure 10: (a) Mean  $\mu_{\text{Tr}[\mathbf{C}]}$  and (b) standard deviation  $\sigma_{\text{Tr}[\mathbf{C}]}$  of the distributions in Fig. 9, shown as a function of  $Re_\lambda$  and  $De$ .

that the dominant last term on the r.h.s. makes the polymers stiff and  $\mathbf{C}$  doesn't stray far away from its equilibrium configuration  $\mathbf{I}$ . On the contrary, the other limit of  $De \rightarrow \infty$  implies a weak restoring force, allowing  $\mathbf{C}$  to grow to large values. Evidently, polymers are stretched by the local velocity gradients given by the first two terms on the r.h.s of Eq. (2.1b).

We plot the pdfs of  $\text{Tr}[\mathbf{C}]$  for different  $Re_\lambda$  in Fig. 9. We first note that although polymers described by the Oldroyd-B model are infinitely stretchable, they can only do so in the presence of very large and sustained velocity gradients. This is confirmed by the very fast decay of the tails of the  $\text{Tr}[\mathbf{C}]$ -pdfs in Fig. 9, clearly suggesting that the polymer lengths always remain bounded in our simulations. Fig. 9(a) shows that, at large  $Re_\lambda$ , the pdfs shift towards the right with increasing  $De$  indicating a larger averaged polymer length. Moreover, the width of the distributions also increases with  $De$ , meaning that polymer lengths also fluctuate over a wider range. This is more accurately shown by Fig. 10 where we plot the mean ( $\mu_{\text{Tr}[\mathbf{C}]}$ ) and standard deviation ( $\sigma_{\text{Tr}[\mathbf{C}]}$ ) of the distributions as a function of  $Re_\lambda$  and  $De$ . Indeed, the polymer lengths and their fluctuations increase with both  $Re_\lambda$  and  $De$ .

Panels (b) and (c) in Fig. 9 show the  $\text{Tr}[\mathbf{C}]$  distributions for smaller  $Re_\lambda$ . With decreasing  $Re_\lambda$ , turbulence intensity decreases and the velocity gradients become weaker on an average and stretch the polymers less (as can be seen from Eq. (2.1b)). Therefore, the mean polymer lengths decrease with decreasing  $Re_\lambda$  as the pdfs shift towards smaller values of  $\text{Tr}[\mathbf{C}]$ . Moreover, polymers are also limited in their maximum extensions as  $Re_\lambda$  decreases. At

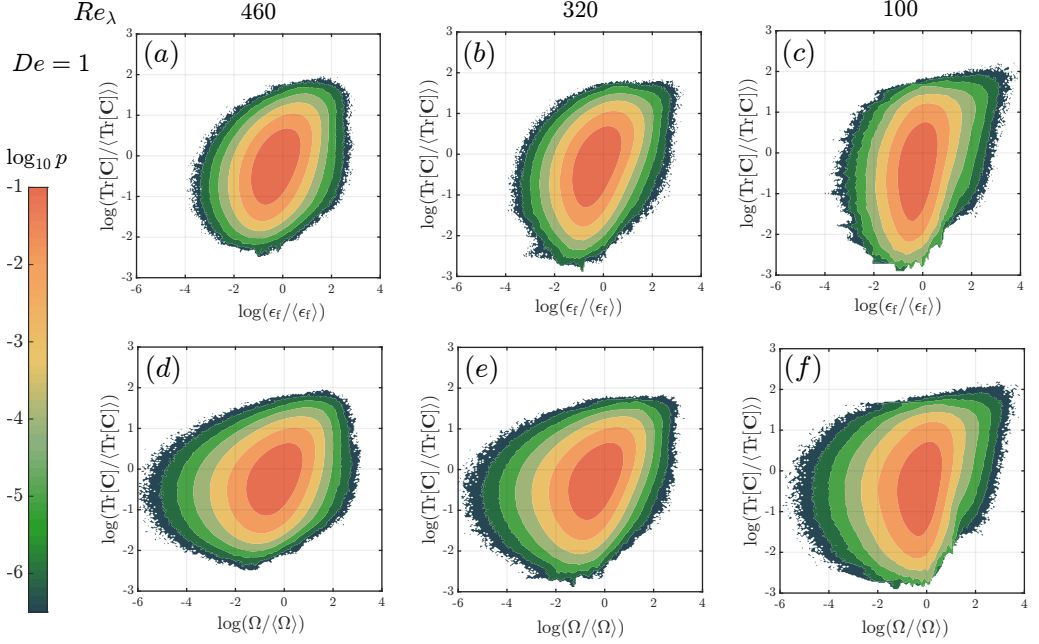


Figure 11: The plot of the joint distributions of the polymer lengths on log-log scale with the (top) dissipation rate  $\epsilon_f$  and (bottom) enstrophy  $\Omega$ , for different  $Re_\lambda$  with  $De \approx 1$ . The color bar shows the color coding of the logarithm of probability  $\log_{10} p$ .

the smallest  $Re_\lambda$ , the velocity gradients are unable to stretch the stiff, small  $De$  polymers considerably. This is captured in Fig. 9(c), where the  $\text{Tr}[\mathbf{C}]$ -pdfs fall-off very fast at small  $De$  showing that polymer lengths have rather small fluctuations. (This also implies that polymer stresses remain very small so that the flow remains laminar for  $De < 1$ ). However, for a large enough  $De (\approx 1)$ , polymers stretch to considerably long lengths, and the resulting large fluctuations are enough to excite sub-dominant velocity fluctuations which gives rise to ET with  $E(k) \sim k^{-4}$  (see Fig. 2).

The above discussion is largely based on how polymers with different  $De$  are stretched by carrier flows at different  $Re_\lambda$ . To understand this better, we now discuss how the polymer stretching  $\text{Tr}[\mathbf{C}]$  is correlated with the velocity gradients  $A_{ij}(\mathbf{x}, t) \equiv \partial_i u_j(\mathbf{x}, t)$  in the flow. To this end, we first decompose  $A_{ij}$  into its symmetric  $S_{ij}$  and antisymmetric  $\omega_{ij}$  components that respectively capture the purely extensional (compressional) and the purely rotational contributions. The squared magnitude of these components are given by the fluid dissipation rate  $\epsilon_f$  and enstrophy  $\Omega$ :

$$\begin{aligned} \Omega &= \omega_{ij}\omega_{ij} ; & \epsilon_f &= 2\nu S_{ij}S_{ij}, \\ \text{where } \omega_{ij} &= (\partial_i u_j - \partial_j u_i) / 2 ; & S_{ij} &= (\partial_i u_j + \partial_j u_i) / 2. \end{aligned} \quad (3.25)$$

The presence of the symmetric term  $\mathbf{C}\nabla\mathbf{u} + (\nabla\mathbf{u})^T\mathbf{C} = 2C_{ik}S_{kj}$  in Eq. (2.1b) means that the extensional (compressional) regions of the flow are directly responsible for the stretching (relaxation) of the polymers. On the other hand, the absence of any  $\omega_{ij}$  terms means that there is no direct effect of the rotation in changing the lengths of polymers. However, turbulence in three-dimensions is marked by the stretching and intensification of vorticity in the direction of local velocity gradients. So, the vortical regions can be expected to correlate with large polymer lengths, although to a lesser degree than the straining regions.

To illustrate the above, we show in Fig. 11 the joint probability distributions (jpdfs) of the

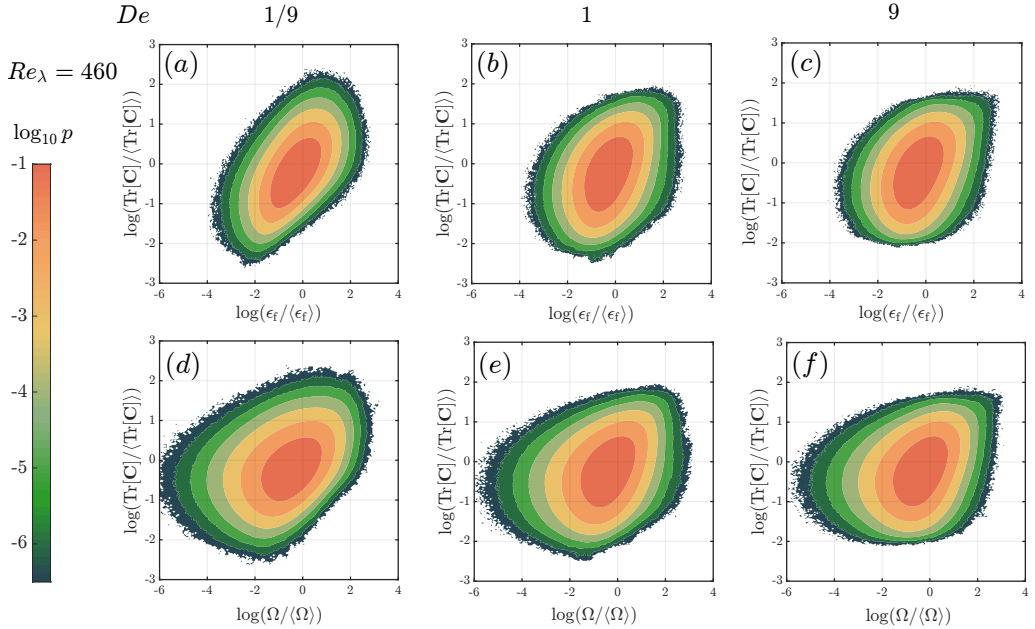


Figure 12: Joint distributions of the polymer lengths with the (top)  $\epsilon_f$  and (bottom)  $\Omega$ , for different  $De$  at  $Re_\lambda \approx 460$ . Different colors correspond to the logarithm of probability  $\log_{10} p$  as coded by the colorbar.

polymer lengths (given by  $\text{Tr}[\mathbf{C}]$ ) with the local stretching rates (given by  $\epsilon_f$ ) as a function of  $Re_\lambda$  for one instance of polymer elasticity of  $De = 1$  in the top panel. We observe that the longest end-to-end lengths of the polymers indeed coincide with the largest stretching rates, while the smallest polymers are found in regions of the flow with small extensional rates. This results in a perceivable tilt of the joint distribution in panel (a). With decreasing  $Re_\lambda$ , the mean lengths of the polymers decreases (see Fig. 10) and their preference for regions with small scale fluctuations increases. This is evident from Fig. 11(b,c) where elongated bottom tails of the jpdfs imply small polymers lengths are more probable at smaller  $Re_\lambda$ . While we still have that the largest polymer extensions coincide with the largest velocity gradients, the core of the jpdfs is now more vertical which indicates that much larger extensions are now possible at even the average stretching rates. This hints towards a decreasing degree of correlation between extreme stretching rates and polymer stretching as  $Re_\lambda$  is reduced.

The bottom panel of Fig. 11 shows the jpdfs of  $\text{Tr}[\mathbf{C}]$  and enstrophy  $\Omega$ . At large  $Re_\lambda$ , large polymer lengths also coincide with extreme vorticity regions. This means polymers are also stretched in regions of large vorticity (similar to what observed for long, polymer-like fibres in Picardo *et al.* (2020)). The maximum enstrophy regions, however, are more likely to have polymers with close to average lengths, implied by Fig. 11(d), unlike the straining regions whose extremes see maximally extended polymers. More importantly, polymers are likely to be stretched even in regions with very small  $\Omega$  as suggested by the left bulge of the jpdfs. This shows that the polymer stretching–enstrophy correlation is not as strong as the stretching–straining correlation. This is even more evident with decreasing  $Re_\lambda$  as vortex stretching becomes progressively weaker. Indeed, panel (f) shows that polymer lengths are rather uniformly distributed, especially for small enstrophy, indicating an even less correlation with polymer stretching.

Fig. 12 shows instead how polymer stretching correlates with the local stretching (top panel) and rotation rates (bottom panel) of the flow, as a function of polymer elasticity. It

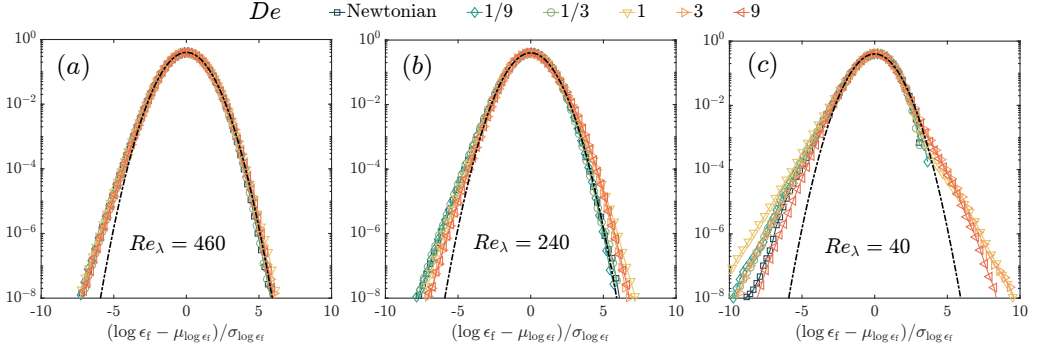


Figure 13: The pdf of the fluid energy dissipation rate  $\epsilon_f$ , compared to a log-normal distribution, for different  $De$  and  $Re_\lambda$ . At (a)  $Re_\lambda \approx 460$ , polymer elasticity has no influence on the intermittent nature of the distributions. However at smaller (b)  $Re_\lambda \approx 240$ , the presence of large  $De$  polymers leads to more large deviations, which are even more prominent at (c)  $Re_\lambda \approx 40$ .

was already shown that large  $De$  polymers stretch more and is clearly captured by their mean lengths in Fig. 10. At small  $De$ , polymers are relatively stiff and have small relaxation times. Therefore, while they are stretched by regions with very large stretching rates, those regions have rather small lifetimes (a quick estimate gives  $\tau \sim S_{ij}^{-1}$ ). So, maximally stretched, stiff polymers are more likely to persist for longer in regions with moderate stretching rates. This means that the maximum of  $\text{Tr}[\mathbf{C}]$  coincides with only slightly larger than the average values of  $\langle \epsilon_f \rangle$ . However, at larger  $De$ , polymers are more stretchable and easily acquire their maximal lengths upon encountering strong straining regions (similar to the observation in Singh (2024) that long, elastic, polymer-like fibres preferentially sample straining regions). At these large  $De$ , polymers remain stretched for longer times so that the fluctuations about the mean become smaller, across all values of  $\epsilon_f$ , thus giving the jpdfs more rounded contours. The bottom panel of Fig. 12 plots the  $\text{Tr}[\mathbf{C}] - \Omega$  joint distributions. We, of course, again have a much wider spread of the distributions compared to  $\text{Tr}[\mathbf{C}] - \epsilon_f$ , yet again suggesting that enstrophy and polymer stretching are less correlated compared to  $\epsilon_f - \text{Tr}[\mathbf{C}]$ , as polymers can also be stretched when enstrophy is very small. Thus, while the maximally stretched polymers are most likely found in regions with maximal enstrophy at large  $De$ , they also tend to be stretched in regions with very small  $\Omega$  when  $De$  is large.

### 3.8. Energy dissipation

In this last section, we discuss how the nature of energy dissipation in turbulence is modified in the presence of polymers. In polymeric flows, energy is dissipated away by both the carrier fluid  $\epsilon_f$  and the dissolved polymers  $\epsilon_p$ . The positive definite fluid dissipation is given by  $\epsilon_f = 2\nu S_{ij}S_{ij}$ , whereas the positive definite polymeric dissipation is related to the average end-to-end polymer length by  $\epsilon_p = (\mu_p/2\tau_p^2) \langle \text{Tr}[\mathbf{C}] - 3 \rangle$ . Both these relations can be readily obtained by multiplying Eq. (2.1a) with  $\mathbf{u}$ , and using Eq. (2.1b) as follows:

$$\begin{aligned} \partial_t \langle \mathbf{u}^2 \rangle / 2 &= \nu \langle \mathbf{u} \nabla^2 \mathbf{u} \rangle + \frac{\mu_p}{\tau_p} \langle \mathbf{u} \cdot \nabla \cdot \mathbf{C} \rangle = -\nu \langle (\nabla \mathbf{u})^2 \rangle - \frac{\mu_p}{\tau_p} \langle \text{Tr}[\mathbf{C} \nabla \mathbf{u}] \rangle + \langle \mathbf{F} \cdot \mathbf{u} \rangle \\ \implies 0 &= -2\nu \langle S_{ij}S_{ij} \rangle - \frac{\mu_p}{\tau_p} \langle \text{Tr}[\mathbf{C} \nabla \mathbf{u}] \rangle + \langle \mathbf{F} \cdot \mathbf{u} \rangle = -\epsilon_f - \epsilon_p + \epsilon_i. \end{aligned} \quad (3.26)$$

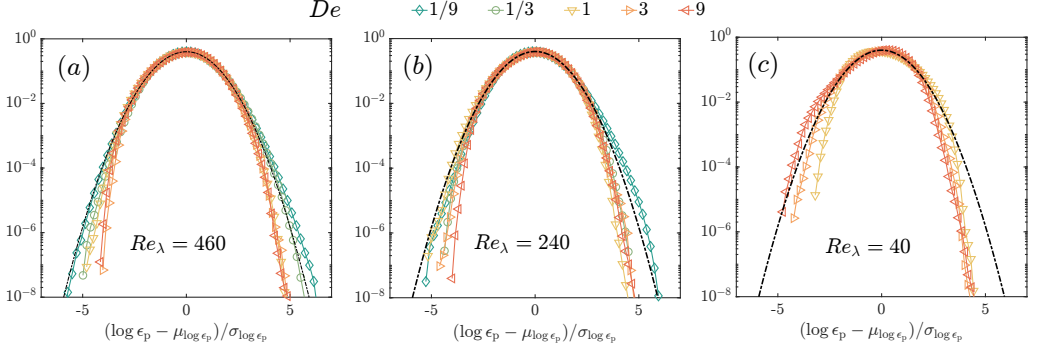


Figure 14: The pdf of the logarithm of polymer dissipation  $\epsilon_p \propto \text{Tr}[\mathbf{C}]$ , as a function of  $De$  for different  $Re_\lambda$  given in the panels. The black dashed curve shows a log-normal distribution for reference. The polymer dissipation becomes less intermittent with increasing  $De$ .

Similarly,

$$\begin{aligned} \mu_p \partial_t \langle \mathbf{C} \rangle &= \mu_p \langle \mathbf{C} (\nabla \mathbf{u}) \rangle + \mu_p \langle (\nabla \mathbf{u})^T \mathbf{C} \rangle - \frac{\mu_p}{\tau_p} \langle \mathbf{C} - \mathbf{I} \rangle \\ \implies 0 &= \frac{2\mu_p}{\tau_p} \langle \text{Tr}[\mathbf{C} \nabla \mathbf{u}] \rangle - \frac{\mu_p}{\tau_p} \langle \text{Tr}[\mathbf{C}] - 3 \rangle \implies \epsilon_p = \frac{\mu_p}{2\tau_p^2} \langle \text{Tr}[\mathbf{C}] - 3 \rangle, \end{aligned} \quad (3.27)$$

where we have used stationarity, periodicity and incompressibility to set time derivatives, fluid non-linearity, pressure contribution and polymer advection terms to zero. The positive-definiteness of  $\epsilon_f$  and  $\epsilon_p$  means that the total energy injected by the forcing  $\epsilon_f$  is dissipated away by both polymers and the fluid in a stationary state. The internal energy of the polymers is proportional to their instantaneous extension so that elongated polymers dissipate away energy as they relax. We now discuss the nature of these measures of dissipation in our polymeric flows.

We first recall that  $\epsilon_f$  in HIT has a distribution whose tails deviate from a log-normal behaviour, in contradiction to the [Kolmogorov \(1962\)](#) prediction. We now show in Fig. 13(a) that the normalised  $\log(\epsilon_f)$ -pdfs remain largely unaffected by the addition of polymers in flows at large  $Re_\lambda$ . The curves for different  $De$  all collapse over the Newtonian curve in Fig. 13(a) which shows that spatio-temporal fluctuations in energy dissipation are unaffected by the addition of polymers. Polymer stresses, though present, do not result in yet larger deviations which are still dominated by the fluid non-linearity. (Note that the mean fluid dissipation  $\langle \log \epsilon_f \rangle$  is still a function of  $De$ .) At a smaller  $Re_\lambda \approx 240$ , the Newtonian curve shows an even larger deviation from log-normality, especially at the left tails, suggesting that dissipation field now has relatively more quiescent regions. There is no appreciable change in the distributions upon the addition of small  $De$  polymers as the polymer stresses remain small. However, when  $De$  is large, elastic effects become appreciable compared to the weakened fluid non-linearity. The polymer stresses are now large enough to create significant fluctuations in the flow so that now there are less quiescent regions and more extreme events. This is apparent from the shrinking left tails and the widening right tails at  $De = 1, 3$  in Fig. 13(b). Curiously, at the largest  $De = 9$ , when the elastic effects begin to weaken again, the large deviations are reduced (this is in parallel to the weakened elastic effects resulting in the shrinking *polymeric* range in Fig. 2(b)). These effects are most clearly seen at the smallest  $Re_\lambda = 40$  where fluid non-linearity does not play a role (and decays exponentially in scales, see Fig. 5(c)). The fluctuations in velocity gradients, therefore, only result from the strong polymer stresses

at large  $De$  and are manifested in the wide-tailed, super log-normal distributions of  $\epsilon_p$  in Fig. 13(c). However, for a large polymer elasticity such as  $De = 9$ , a weakening of elastic effects results in a mild shrinking of the tails of the pdf.

We show the distributions of the polymer dissipation  $\epsilon_p$  in Fig. 14, which are sub-log-normal, unlike  $\epsilon_f$ , thus indicating a significantly less intermittent behaviour. In particular, at small  $De$ ,  $\epsilon_p$  shows more large deviations. These stiff polymers rarely stretch and even when stretched, they quickly relax back to their small, equilibrium lengths. This means any deviations about a small mean are more significant. Thus, the polymer dissipation  $\epsilon_p \propto \text{Tr}[\mathbf{C}]$  shows the widest tails at the smallest  $De = 1/9$ , which are wider than even a log-normal distribution, especially at larger  $Re_\lambda$ 's in Fig. 14(a,b). With increasing  $De$  polymers tend to stretch more and for longer duration owing to the larger relaxation times. Thus, fluctuations in lengths become less important at large  $De$ , and consequently, the stored energy is dissipated away in a more uniform and less intermittent manner, with fewer large deviations. This results in the log  $\epsilon_p$  distributions becoming progressively sub-lognormal. This effect is rather persistent across all  $Re_\lambda$ , even into the ET regime at  $Re_\lambda \approx 40$ , as seen from Fig. 14.

#### 4. Conclusions

In this work, we investigate how various measures that typically characterise classical, Newtonian turbulence behave in polymeric flows as both elasticity and inertia of the flow are varied. While turbulence statistics indeed depend on both  $Re$  and  $De$ , which quantify fluid inertia and polymer elasticity, respectively, we show that the addition of polymers has contrasting effects on different turbulence statistics.

We begin by showing that the energy spectrum in polymeric flows shows a multiscaling nature, especially at large  $Re$  and moderate  $De$ , where three different dominant flux contributions—viz. fluid non-linearity, polymeric and the dissipative contributions—lead to three distinct scaling exponents. This multiscaling behaviour is invariably lost at both very large and very small polymer elasticity, where instead the Newtonian behaviour is recovered similar to the observation by [Rosti \*et al.\* \(2023\)](#). With decreasing  $Re_\lambda$ , the Newtonian and polymeric regimes are progressively lost as the fluid inertia weakens and viscosity becomes more important. A unique, smooth, dissipative, elastic turbulence regime spans a wide range of scales at very small  $Re_\lambda$ , when polymer elasticity is large. We further shed light on the dynamics of our polymeric flows by estimating the typical life-times of velocity fluctuations, and the rates of energy transfer to smaller fluid scales and to the polymeric mode. We use scaling arguments to show that the classical fluid energy cascade is slowed and weakened in the presence of polymers. The real space statistics of velocity fluctuations, captured by the structure functions, also admit different scaling exponents that are directly related to the Fourier space scaling of the energy spectra.

The real space statistics also additionally reveal the intermittent nature of velocity fluctuations in polymeric flows. At very large  $Re_\lambda$ , the presence of polymers has almost no effect on the kurtosis of fluctuations. However, with decreasing  $Re_\lambda$ , elastic stresses become increasingly more important than the fluid non-linearity and result in strongly intermittent velocity fluctuations. The relative importance of polymer stresses is made clear by the end-to-end polymer lengths which is given by the trace of the conformation tensor. As expected, polymers stretch more as their elasticity increases and they are able to span a wide range of scales. We further study how polymers stretch in different regions of the flow by decomposing velocity gradients into extensional and rotational components. Extensional regions, quantified by the symmetrised velocity gradients, promote the stretching of the polymers, whereas the local rotation rates, quantified by enstrophy, play a rather indirect role in their stretching. While we indeed find that local rotation rates correlate with large polymer lengths, since

velocity gradients intensify vorticity by stretching them in their direction, polymers are shown to also stretch in regions with small rotation rates, thus indicating a lesser correlation between enstrophy and polymer lengths.

Finally, we relate polymer lengths and velocity gradients to the energy dissipated away by the carrier fluid and the polymers, and compare them to a log-normal distribution. At large  $Re_\lambda$ , much like the kurtosis of velocity fluctuation, fluctuations of fluid dissipation remains unchanged upon the addition of polymers. However, polymer stresses become important at small  $Re_\lambda$  and result in large deviations in fluid dissipation. The effect of polymers is most clear at the smallest  $Re_\lambda$  where the fluid non-linearity is inactive and yet the fluid dissipation distribution is very far from log-normal. On the other hand, dissipation by polymers themselves is much less intermittent compared to the fluid dissipation, with tails shrinking even further as polymer elasticity increases. This is because polymers are able to stretch more uniformly and hence dissipate away their stored energy in a less intermittent, more uniform fashion.

With this work, we have connected polymeric turbulence at large Reynolds number with elastic turbulence, where inertia effects are vanishing. While the two regimes show substantial differences, as for example clearly indicated by the different multiscaling behaviour of the energy spectra, the transition between the two is rather smooth and continuous in the chosen framework of homogeneous and isotropic turbulence. Future work should deal with better characterising and explaining the origin of the various identified exponents of the energy spectra, as well as extending the analysis to more complex flows.

**Acknowledgements.** The research was supported by the Okinawa Institute of Science and Technology Graduate University (OIST) with subsidy funding to M.E.R. from the Cabinet Office, Government of Japan. M.E.R. also acknowledges funding from the Japan Society for the Promotion of Science (JSPS), grants 24K00810 and 24K17210. The authors acknowledge the computer time provided by the Scientific Computing & Data Analysis section of the Core Facilities at OIST, and the computational resources provided by the HPCI System (Project IDs: hp230018, hp220099, hp210269, and hp210229). R.K.S. thanks Alessandro Chiarini (OIST) for discussions and suggestions.

**Declaration of interests.** The authors report no conflict of interest.

## REFERENCES

- BAGHERI, FARANGGIS, MITRA, DHRUBADITYA, PERLEKAR, PRASAD & BRANDT, LUCA 2012 Statistics of polymer extensions in turbulent channel flow. *Phys. Rev. E* **86**, 056314.
- BALCI, NUSRET, THOMASES, BECCA, RENARDY, MICHAEL & DOERING, CHARLES R. 2011 Symmetric factorization of the conformation tensor in viscoelastic fluid models. *Journal of Non-Newtonian Fluid Mechanics* **166** (11), 546–553, xVIth International Workshop on Numerical Methods for Non-Newtonian Flows.
- BENZI, ROBERTO, DE ANGELIS, ELISABETTA, GOVINDARAJAN, RAMA & PROCACCIA, ITAMAR 2003 Shell model for drag reduction with polymer additives in homogeneous turbulence. *Phys. Rev. E* **68**, 016308.
- BERMAN, N S 1978 Drag reduction by polymers. *Annual Review of Fluid Mechanics* **10** (Volume 10, 1978), 47–64.
- BERTI, S., BISTAGNINO, A., BOFFETTA, G., CELANI, A. & MUSACCHIO, S. 2008 Two-dimensional elastic turbulence. *Phys. Rev. E* **77**, 055306.
- BERTI, S. & BOFFETTA, G. 2010 Elastic waves and transition to elastic turbulence in a two-dimensional viscoelastic kolmogorov flow. *Phys. Rev. E* **82**, 036314.
- BHATTACHARJEE, J. K. & THIRUMALAI, D. 1991 Drag reduction in turbulent flows by polymers. *Phys. Rev. Lett.* **67**, 196–199.
- CAI, W.-H., LI, F.-C. & ZHANG, H.-N. 2010 Dns study of decaying homogeneous isotropic turbulence with polymer additives. *Journal of Fluid Mechanics* **665**, 334–356.
- CHOUËIRI, GEORGE H., LOPEZ, JOSE M. & HOF, BJÖRN 2018 Exceeding the asymptotic limit of polymer drag reduction. *Phys. Rev. Lett.* **120**, 124501.

- DE LILLO, F., BOFFETTA, G. & MUSACCHIO, S. 2012 Control of particle clustering in turbulence by polymer additives. *Phys. Rev. E* **85**, 036308.
- DEN TOONDER, J. M. J., HULSEN, M. A., KUIKEN, G. D. C. & NIEUWSTADT, F. T. M. 1997 Drag reduction by polymer additives in a turbulent pipe flow: numerical and laboratory experiments. *Journal of Fluid Mechanics* **337**, 193–231.
- VAN DOORN, ERIC, WHITE, CHRISTOPHER M. & SREENIVASAN, K. R. 1999 The decay of grid turbulence in polymer and surfactant solutions. *Physics of Fluids* **11** (8), 2387–2393.
- DUBIEF, YVES, TERRAPON, VINCENT E. & HOF, BJÖRN 2023 Elasto-inertial turbulence. *Annual Review of Fluid Mechanics* **55** (1), 675–705.
- DUBIEF, YVES, TERRAPON, VINCENT E. & SORIA, JULIO 2013 On the mechanism of elasto-inertial turbulence. *Physics of Fluids* **25** (11).
- ESCUDIER, M.P, PRESTI, F & SMITH, S 1999 Drag reduction in the turbulent pipe flow of polymers. *Journal of Non-Newtonian Fluid Mechanics* **81** (3), 197–213.
- FRISCH, U 1996 *Turbulence: The Legacy of A. N. Kolmogorov*. Cambridge University Press.
- GILLISSEN, J. J. J. 2008 Polymer flexibility and turbulent drag reduction. *Phys. Rev. E* **78**, 046311.
- GILLISSEN, J. J. J. 2021 Weakened energy cascade in elastoinertial turbulence. *Phys. Rev. E* **103**, 063108.
- GROISMAN, A. & STEINBERG, V. 1998 Elastic vs. inertial instability in a polymer solution flow. *Europhysics Letters* **43** (2), 165.
- GROISMAN, A. & STEINBERG, V. 2000 Elastic turbulence in a polymer solution flow. *Nature* **405** (6782), 53–55.
- GROISMAN, ALEXANDER & STEINBERG, VICTOR 2001 Efficient mixing at low reynolds numbers using polymer additives. *Nature* **410** (6831), 905–908.
- GROISMAN, ALEXANDER & STEINBERG, VICTOR 2004 Elastic turbulence in curvilinear flows of polymer solutions. *New Journal of Physics* **6** (1), 29.
- GUPTA, ANUPAM & VINCENZI, DARIO 2019 Effect of polymer-stress diffusion in the numerical simulation of elastic turbulence. *Journal of Fluid Mechanics* **870**, 405–418.
- HINCH, E. J. 1977 Mechanical models of dilute polymer solutions in strong flows. *The Physics of Fluids* **20** (10), S22–S30.
- IZBASSAROV, DAULET, ROSTI, MARCO E., ARDEKANI, M. NIAZI, SARABIAN, MOHAMMAD, HORMOZI, SARAH, BRANDT, LUCA & TAMMISOLA, OUTI 2018 Computational modeling of multiphase viscoelastic and elastoviscoplastic flows.
- KALELKAR, CHIRAG, GOVINDARAJAN, RAMA & PANDIT, RAHUL 2005 Drag reduction by polymer additives in decaying turbulence. *Phys. Rev. E* **72**, 017301.
- KIM, J & MOIN, P 1985 Application of a fractional-step method to incompressible navier-stokes equations.
- KOLMOGOROV, A. N. 1941 Dissipation of energy in the locally isotropic turbulence. *Dokl. Akad. Nauk. SSSR* **32**, 19–21.
- KOLMOGOROV, A. N. 1962 A refinement of previous hypotheses concerning the local structure of turbulence in a viscous incompressible fluid at high reynolds number. *J. Fluid Mech.* **13** (1), 82–85.
- LARSON, R. G. 1992 Instabilities in viscoelastic flows. *Rheologica Acta* **31** (3), 213–263.
- LEWY, THEO & KERSWELL, RICH 2024 Revisiting 2d viscoelastic kolmogorov flow: A centre-mode-driven transition , arXiv: 2410.07402.
- LI, DONG-YANG, ZHANG, HONGNA, CHENG, JIAN-PING, LI, XIAO-BIN, LI, FENG-CHEN, QIAN, SHIZHI & JOO, SANG WOO 2017 Numerical simulation of heat transfer enhancement by elastic turbulence in a curvy channel. *Microfluidics and Nanofluidics* **21** (2), 25.
- LUMLEY, J. L. 1973 Drag reduction in turbulent flow by polymer additives. *Journal of Polymer Science: Macromolecular Reviews* **7** (1), 263–290.
- L'VOV, VICTOR S., POMYALOV, ANNA, PROCACCIA, ITAMAR & TIBERKEVICH, VASIL 2004 Drag reduction by polymers in wall bounded turbulence. *Phys. Rev. Lett.* **92**, 244503.
- NGUYEN, M. QUAN, DELACHE, ALEXANDRE, SIMOËNS, SERGE, BOS, WOUTER J. T. & EL HAJEM, MAMOUD 2016 Small scale dynamics of isotropic viscoelastic turbulence. *Phys. Rev. Fluids* **1**, 083301.
- PAN, L., MOROZOV, A., WAGNER, C. & ARRATIA, P. E. 2013 Nonlinear elastic instability in channel flows at low reynolds numbers. *Phys. Rev. Lett.* **110**, 174502.
- PERLEKAR, PRASAD, MITRA, DHRUBADITYA & PANDIT, RAHUL 2006 Manifestations of drag reduction by polymer additives in decaying, homogeneous, isotropic turbulence. *Phys. Rev. Lett.* **97**, 264501.
- PERLEKAR, PRASAD, MITRA, DHRUBADITYA & PANDIT, RAHUL 2010 Direct numerical simulations of statistically steady, homogeneous, isotropic fluid turbulence with polymer additives. *Phys. Rev. E* **82**, 066313.

- PICARDO, JASON R., SINGH, RAHUL, RAY, SAMRIDDIH SANKAR & VINCENZI, DARIO 2020 Dynamics of a long chain in turbulent flows: impact of vortices. *Philosophical Transactions of the Royal Society A: Mathematical, Physical and Engineering Sciences* **378** (2175), 20190405.
- PROCACCIA, ITAMAR, L'VOV, VICTOR S. & BENZI, ROBERTO 2008 Colloquium: Theory of drag reduction by polymers in wall-bounded turbulence. *Rev. Mod. Phys.* **80**, 225–247.
- PTASINSKI, P. K., BOERSMA, B. J., NIEUWSTADT, F. T. M., HULSEN, M. A., VAN DEN BRULE, B. H. A. A. & HUNT, J. C. R. 2003 Turbulent channel flow near maximum drag reduction: simulations, experiments and mechanisms. *Journal of Fluid Mechanics* **490**, 251–291.
- PTASINSKI, P. K., NIEUWSTADT, F. T. M., VAN DEN BRULE, B. H. A. A. & HULSEN, M. A. 2001 Experiments in turbulent pipe flow with polymer additives at maximum drag reduction. *Flow, Turbulence and Combustion* **66** (2), 159–182.
- QIN, BOYANG & ARRATIA, PAULO E. 2017 Characterizing elastic turbulence in channel flows at low reynolds number. *Phys. Rev. Fluids* **2**, 083302.
- RAY, SAMRIDDIH SANKAR & VINCENZI, DARIO 2016 Elastic turbulence in a shell model of polymer solution. *Europhysics Letters* **114** (4), 44001.
- ROSTI, MARCO E., PERLEKAR, PRASAD & MITRA, DHRUBADITYA 2023 Large is different: Nonmonotonic behavior of elastic range scaling in polymeric turbulence at large reynolds and Deborah numbers. *Science Advances* **9** (11), eadd3831.
- ROTA, GIULIO FOGGI, AMOR, CHRISTIAN, CLAINCHE, SOLEDAD LE & ROSTI, MARCO EDOARDO 2024 A unified view of elastic and elasto-inertial turbulence in channel flows , arXiv: 2310.05340.
- SAMANTA, DEVRANJAN, DUBIEF, YVES, HOLZNER, MARKUS, SCHÄFER, CHRISTOF, MOROZOV, ALEXANDER N., WAGNER, CHRISTIAN & HOF, BJÖRN 2013 Elasto-inertial turbulence. *Proceedings of the National Academy of Sciences* **110** (26), 10557–10562.
- SHAQFEH, E S G 1996 Purely elastic instabilities in viscometric flows. *Annual Review of Fluid Mechanics* **28** (1), 129–185.
- SINGH, RAHUL K. 2024 Elasticity of fibres prefers the chaos of turbulence , arXiv: 2406.06033.
- SINGH, RAHUL K., PERLEKAR, PRASAD, MITRA, DHRUBADITYA & ROSTI, MARCO E. 2024 Intermittency in the not-so-smooth elastic turbulence. *Nature Communications* **15** (1), 4070.
- SREENIVASAN, K. R. & WHITE, C. M. 2000 The onset of drag reduction by dilute polymer additives, and the maximum drag reduction asymptote. *Journal of Fluid Mechanics* **409**, 149–164.
- SUGIYAMA, KAZUYASU, II, SATOSHI, TAKEUCHI, SHINTARO, TAKAGI, SHU & MATSUMOTO, YOICHIRO 2011 A full eulerian finite difference approach for solving fluid–structure coupling problems. *Journal of Computational Physics* **230** (3), 596–627.
- TABOR, M. & DE GENNES, P. G. 1986 A cascade theory of drag reduction. *Europhysics Letters* **2** (7), 519.
- TOMS, B. A. 1948 Some observations on the flow of linear polymer solutions through straight tubes at large reynolds numbers. *Proc. 1st Int. Cong. Rheology, Amsterdam, 1948* **135**.
- TOMS, B. A. 1977 On the early experiments on drag reduction by polymers. *The Physics of Fluids* **20** (10), S3–S5.
- VALENTE, P. C., DA SILVA, C. B. & PINHO, F. T. 2016 Energy spectra in elasto-inertial turbulence. *Physics of Fluids* **28** (7).
- VINCENZI, DARIO, JIN, SHI, BODENSCHATZ, EBERHARD & COLLINS, LANCE R. 2007 Stretching of polymers in isotropic turbulence: A statistical closure. *Phys. Rev. Lett.* **98**, 024503.
- VIRK, P. S. 1975 Drag reduction fundamentals. *AIChE Journal* **21** (4), 625–656.
- WHITE, CHRISTOPHER M. & MUNGAL, M GODFREY 2008 Mechanics and prediction of turbulent drag reduction with polymer additives. *Annual Review of Fluid Mechanics* **40** (1), 235–256.
- XI, LI 2019 Turbulent drag reduction by polymer additives: Fundamentals and recent advances. *Physics of Fluids* **31** (12).
- YANG, SHU-QING & DOU, G. 2010 Turbulent drag reduction with polymer additive in rough pipes. *Journal of Fluid Mechanics* **642**, 279–294.
- ZHANG, WEN-HUA, ZHANG, HONG-NA, LI, YU-KE, YU, BO & LI, FENG-CHEN 2021a Role of elasto-inertial turbulence in viscoelastic drag-reducing turbulence. *Physics of Fluids* **33** (8).
- ZHANG, YI-BAO, BODENSCHATZ, EBERHARD, XU, HAITAO & XI, HENG-DONG 2021b Experimental observation of the elastic range scaling in turbulent flow with polymer additives. *Science Advances* **7** (14), eabd3525.